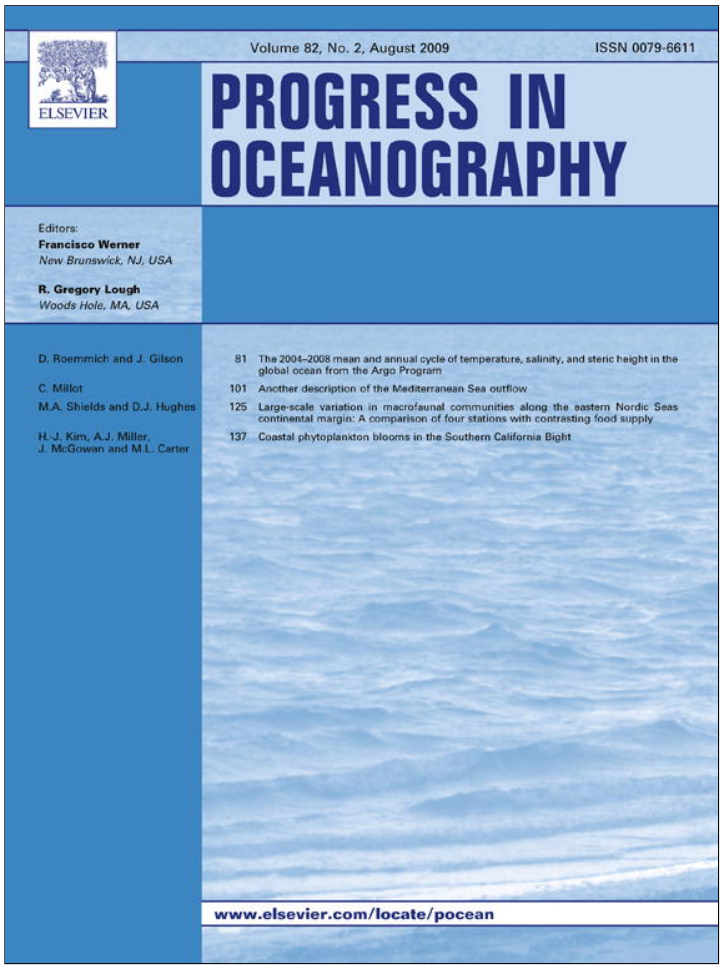

Progress in Oceanography 82 (2009) 101–124

Contents lists available at ScienceDirect

Progress in Oceanography

journal homepage: www.elsevier.com/locate/pocean

# Another description of the Mediterranean Sea outflow

Claude Millot

*Laboratoire d'Océanographie Physique Biogéochimique, Antenne LOPB-COM-CNRS, BP 330, 83150 La Seyne/mer, France*

ARTICLE INFO

*Article history:*
Received 26 February 2008
Received in revised form 13 April 2009
Accepted 14 April 2009
Available online 22 April 2009

*Keywords:*
Mediterranean Sea
Strait of Gibraltar
Circulation
Water masses

ABSTRACT

Papers about the outflow in the Strait of Gibraltar assume that (i) it is composed of only two Mediterranean Waters (MWs), the Levantine Intermediate Water (LIW) and the Western Mediterranean Deep Water (WMDW) from the eastern and western basins, respectively, (ii) both MWs are mixed near 6°W, hence producing a homogeneous outflow that is then split into veins, due to its cascading along different paths and to different mixing conditions with the Atlantic Water (AW).

A re-analysis of 1985–1986 CTD profiles (Gibraltar Experiment) indicates two other MWs, the Winter Intermediate Water (WIW) from the western basin and the Tyrrhenian Dense Water (TDW) basically originated from the eastern basin. In the central Alboran subbasin, these four MWs are clearly differentiated, roughly lying one above the other in proportions varying from north to south. Proportions also vary with time, so that the outflow can be mostly of either eastern or western origin. While progressing westward, the MWs can still be differentiated and associated isopycnals tilt up southward as much as being, in the sill surroundings, roughly parallel to the Moroccan continental slope where the densest MWs are. The MWs at the sill are thus juxtaposed and they all mix with AW, leading to an outflow that is horizontally heterogeneous just after the sill (5°45′W) before progressively becoming vertically heterogeneous as soon as 6°15′W. There can be little LIW and/or no WMDW outflowing for a while.

An analysis of new 2003–2008 time series from two CTDs moored (CIESM Hydro-Changes Programme) at the sill (270 m) and on the Moroccan shelf (80 m) confirms the juxtaposition of the MWs, their individual and generally intense mixing with AW, as well as the large temporal variability of the outflow composition. Only LIW and TDW were indicated at the sill while, on the shelf, only LIW, TDW sometimes denser there than ~200 m below, and WMDW were indicated; but none of the MWs has been permanently outflowing at one or the other place.

The available data can be analyzed coherently. Intermediate and deep MWs are formed in both basins in amounts that, although variable from year to year, allow their tracing up to the strait. Four major MWs circulate alongslope counterclockwise as density currents and as long as they are not trapped within a basin, which is necessarily the case for the deep MWs. In the Alboran, the intermediate MWs (WIW, LIW and upper-TDW) circulate in the north while the deep MWs (lower-TDW and WMDW) are uplifted, hence relatively motionless and mainly pushed away in the south. Since both the intermediate and deep MWs outflow at the sill, they are considered as light and dense MWs, the light–dense MWs interface possibly intersecting the AW–MWs interface in the sill surroundings. Considering an outflow east of the sill composed of only two (light–dense) homogeneous layers gives significant results. Across the whole strait, the outflow has spatial and temporal variabilities much larger than previously assumed. The MWs are superposed in the sea and lead at the sill to juxtaposed and vertically stratified suboutflows that will cascade independently before forming superposed veins in the ocean. These veins can have similar densities and hydrographic characteristics even if associated with different MWs, which accounts for the features permanency assumed up to now. The outflow structure downstream of the sill depends on its composition upstream and, more importantly, on that of AW in the sill surroundings where fortnightly and seasonal signals are imposed on the whole outflow.



## 1. Introduction

Papers about the strait of Gibraltar in general, and about the Mediterranean outflow in particular, are based on the same concept. They assume that the outflow is composed of only two out of four major Mediterranean Waters (MWs), and that both are mixed near 6°W, hence producing a homogeneous outflow that is then split into veins, due to its cascading along different paths and to different mixing conditions with the Atlantic Water (AW). This concept is supported neither by the analyses we have been

*E-mail addresses:* f4eut@winlink.org, cmillot@ifremer.fr

0079-6611/$ - see front matter © 2009 Published by Elsevier Ltd.
doi:10.1016/j.pocean.2009.04.016

conducting for a while about the functioning of the Mediterranean Sea nor by those we have recently undertaken about the Strait of Gibraltar itself. Current and personal thoughts are thus presented separately in Sections 1.1 and 1.2, respectively.

### 1.1. Current thoughts

Reliable information about the strait (Fig. 1) has been gathered from some time, and Lacombe and Richez (1982) have first specified its basic functioning, with a surface inflow of fresh Atlantic Water (salinity $S \sim 36$) and a deep outflow of salty Mediterranean Water ($S \sim 38$) that results from evaporation exceeding precipitation and rivers runoff in the sea. They have also emphasized the tremendous role of the internal tide in mixing the water masses and generating small-scale features.

Because they can easily be recognized on nearly all $\theta$–$S$ ($\theta$: potential temperature) diagrams within the western basin of the sea and within the Alboran subbasin (Fig. 2) in particular, the salty and relatively warm Levantine Intermediate Water (LIW), the intermediate water formed in the eastern basin, and the cool and relatively fresh Western Mediterranean Deep Water (WMDW), the deep water formed in the western basin, have generally been considered to be the sole components of the outflow. In a recent review paper, Baringer and Price (1999) consider the outflow to be 90% LIW and 10% WMDW, as formerly proposed by Bryden and Stommel (1984). Such proportions would mean the whole sea forms mainly intermediate water, mainly in the eastern basin, and there, only in the Levantine subbasin. The constancy of these percentages, still generally accepted nowadays, suggests that no attempt has been made to improve or reconsider them.

Assuming an outflow composed of only LIW and WMDW, it was soon recognized (e.g. Bryden et al., 1978; Bryden and Stommel, 1982) that these MWs are found mainly in the north and south of the Alboran, respectively, while pioneering observations (Allain, 1964) mentioned the occurrence of WMDW at Camarinal Sill South (300 m; 5°45′W). The only other MW reported (Gascard and Richez, 1985) to intermittently occur in the western Alboran is the Winter Intermediate Water (WIW), the intermediate water formed in the western basin and that lies above LIW, but this observation has not been considered in subsequent papers. In addition, the possible occurrence, not only in the western Alboran but also in the western basin as a whole, of the deep waters formed in the eastern basin in both the Aegean and the Adriatic has never been mentioned, even though attention has been paid to them through the Eastern Mediterranean Transient (EMT; Roether et al., 1996).

After this series of general-oceanography papers, the development of two-layer hydraulic control simulations motivated new observations during the 1985–1986 Gibraltar Experiment (GE) and turned general interest towards the dynamics of flows through straits, leading to significant progress in their understanding (Bryden and Kinder, 1991). Of particular interest are the numerous and very valuable sets of cross–strait/north–south CTD transects performed using relatively high resolution sampling (2–3 nautical miles (nm) in general, sometimes less), high frequency (few days) and during several campaigns such as LYNCH-702-86, GIB1 and GIB2. We present hereafter our analysis of the GIB1 and GIB2 data mainly and show some LYNCH data west of the sill.

Gascard and Richez (1985) and Kinder and Parrilla (1987) inferred that LIW was found at 200–600 m in the northern 2/3 of the Alboran while WMDW was found below 800 m in the central region (near 36°N) and below 400 m along the African slope. Parrilla et al. (1989) considered that LIW and WMDW have the same distribution and characteristics until almost the sill as they had in the eastern Alboran. Pettigrew (1989) definitely demonstrated the occurrence of WMDW at the sill while Kinder and Parrilla (1987) have shown its presence not only in the southern part of the sill but also few nm west of it. Then, because of active mixing processes (e.g. Wesson and Gregg, 1994), these waters were considered to become a single MW (Parrilla et al., 1989), which has been generally accepted. To our knowledge, comparative analyses of successive north–south transects of $\theta$, $S$ and $\sigma$ (the potential density anomaly), from GE and other experiments as well, have

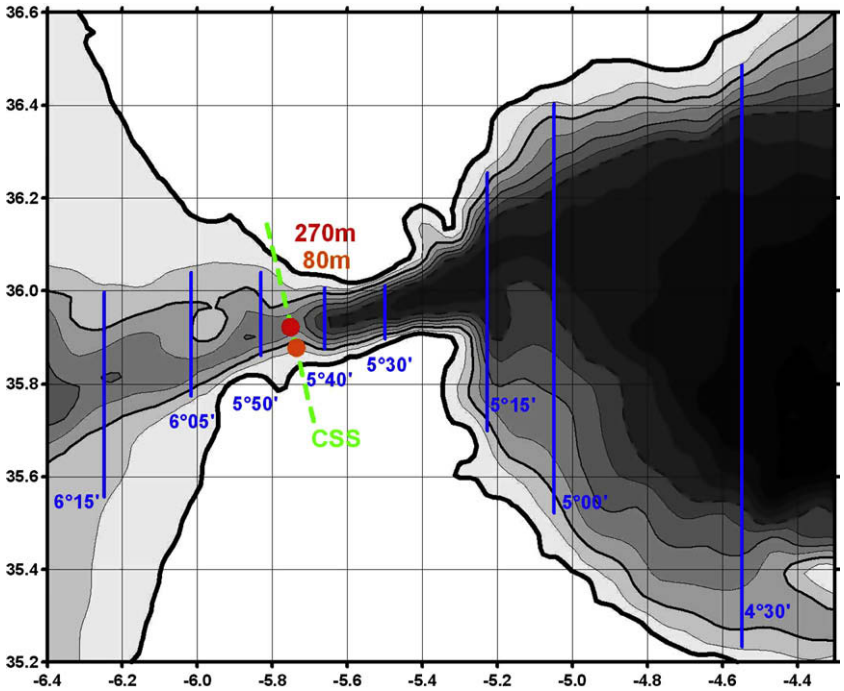


**Fig. 1.** The study area with the schematized GE transects (in blue) together with the HPC 270-m site (red dot, 35°55.2′N–5°45.0′W, on a small plateau ~1.1 km north of the ~300-m deepest part of Camarinal Sill South (CSS, green dashed line)), and the 80-m one (orange dot, 35°52.8′N–5°43.5′W) that are at ~10 and 5 km from the Moroccan coast. (For interpretation of the references to colour in this figure legend, the reader is referred to the web version of this article.)

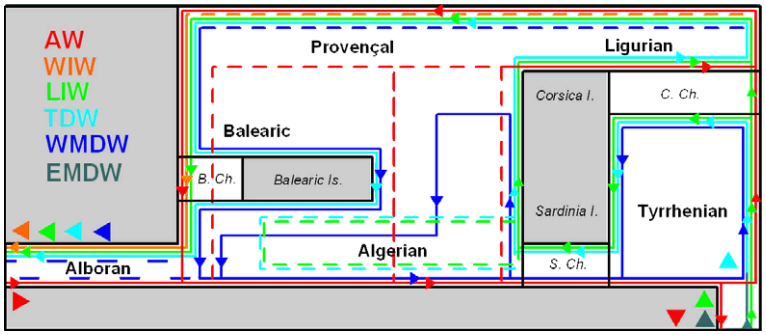


**Fig. 2.** Schematic diagram of the circulation of AW and all major MWs together with the major subbasins, islands and channels in the western basin of the Mediterranean Sea. All waters mainly flowing counterclockwise alongslope are represented by full lines in an on–offshore direction as seen from above. Dashed lines represent (i) for AW its seaward spreading due to the mesoscale Algerian Eddies, (ii) for LIW and TDW their entrainment away from the Sardinian slope by these eddies, (iii) for WIW and WMDW in the north of the basin their zone of formation, (iv) for WMDW in the Alboran its uplifting and relatively low circulation. More details are given in the text, as well as in Millot (1999) and Millot and Taupier-Letage (2005a).

been published mainly for the Gulf of Cadiz (e.g. Ochoa and Bray, 1991; Ambar et al., 2002) and the Alboran (see above). For the strait itself, only Parrilla et al. (1989) inferred general features from transects collected during several campaigns.

Thereafter, and as done by Kinder and Parrilla (1987), authors no longer analyzed cross–strait transects and either inferred or performed along-strait ones. For instance, even thought Bray et al. (1995) considered most of the GE data and described the 3-D characteristics of the AW–MW interface within the strait, they analyzed changes in $\theta$–$S$ diagrams only from west to east, not from north to south. Baringer and Price (1997, 1999) concentrated on the re-analysis of dedicated 1988 data and, considering that LIW and WMDW completely mix within the strait, relied on a unique along-strait CTD transect. The homogeneous outflow assumption at the strait outlet is used in most of the recent simulations of the general circulation at ocean scale (e.g. Wu et al., 2007) and of the exchanges through the strait (e.g. Sannino et al., 2002), as well as in most of the simulations (e.g. Serra and Ambar, 2002; Johnson et al., 2002) and laboratory experiments (e.g. Davies et al., 2002) dedicated to the outflow.

Assuming a homogeneous outflow, it is widely accepted that basic features about its cascading from the sill are linked to its relatively high density and to the Coriolis effect while the gradual attenuation of its anomalously high thermohaline and density properties results from the mixing with the surrounding fresher and cooler AW. As a whole, the outflow then reaches quasi-equilibrium as a density current and flows northward alongslope. At 100–200 km downstream from the strait, it is said to be subdivided into two main veins at 800 and 1200 m (e.g. Siedler, 1968; Madelain, 1970) and a shallower one at 500 m (Howe et al., 1974; Zenk, 1975; Ambar, 1983) while only the two deepest veins were sometimes identified (e.g. Baringer and Price, 1997). At 6°05′W where maximum depths are 400 m, the veins were generally hard to distinguish (e.g. Baringer and Price, 1997; Ambar et al., 1999) while the two densest veins can be identified (400–700 m) at 6°30′W (Borenäs et al., 2002). Following Madelain (1970), the veins have been generally attributed to the bottom topography, canyons having been expected to divert the original homogeneous outflow and cause it to mix differently with AW. Siedler (1968) hypothesized that the tidal mixing temporal variability within the strait could lead to an outflow having alternatively different characteristics, hence mainly forming two veins, while Howe et al. (1974) suggested that the upper vein originates from shallow depth in the strait.

According to north–south transects near 7°W (Ambar and Howe, 1979a,b), the saltiest and coolest water found in the south and the slightly fresher and warmer water found in the north should form the two deepest veins. Most recent surveys (Ambar et al., 2002) have shown that the shallowest vein has relatively high temperatures, while representative $\sigma$ values for the cores of the three veins at their equilibrium depths are 27.4, 27.5 and 27.8 kg m$^{-3}$. In their simulations of the outflow splitting, Borenäs et al. (2002) consider that the two deepest veins at 6°30′W differ by $\Delta\sigma \sim 0.25$ kg m$^{-3}$.

Additionally, Bray et al. (1995) statistically analyzed the whole GE data set. They considered a homogeneous MW and an AW composed of North Atlantic Central Water (NACW, $\theta$ = 12–14 °C, $S$ = 35.5–36.0), said to be found during all campaigns and overlaid by a modified form of NACW named Surface Atlantic Water (SAW, $\theta$ = 16–22 °C, $S$ = 36.0–36.5). They interpreted the $\theta$ and $S$ distributions within the strait as a mixture of these three principal water types and inferred typical percentages for an upper, an interface and a lower layer, as well as seasonal and east–west variations.

### 1.2. Other thoughts

We already mentioned (Millot, 1999; Millot and Taupier-Letage, 2005a) that significant WIW amounts occurred in the Alboran and commented on the importance of the Tyrrhenian Dense Water (TDW) that results from the deep eastern waters cascading into the western basin. The hydrographic characteristics in the sea of AW and the four major MWs are synthesized in Section 1.2.1.

We also described in these papers the AW and MWs circulation in the whole sea and explained why, according to the Coriolis effect, they circulate alongslope counterclockwise as density currents looking like veins, except when they are trapped, as is necessarily the case for the densest part of WMDW in the deepest part of the western basin. A new schematization of the circulation in the western basin is proposed in Section 1.2.2.

Additionally, we specified some aspects of the outflow variability in both the long term (decades; Millot et al., 2006) and the short term (weeks; Millot, 2008). In this last paper we have also shown that the outflow characteristics in the Atlantic depend more on the nature of AW in the sill surroundings than on the outflow composition east of the sill. At medium scales (seasons-years), the role of the MWs–AW mixing in defining the outflow characteristics is made more complex by the large seasonal variability and huge interannual increase of the AW salinity (Millot, 2007). Our own results at Gibraltar are summarized in Section 1.2.3.

#### 1.2.1. The waters hydrographic characteristics

Due to intense mixing in the sill surroundings, the $\theta$ and $S$ extrema that characterize the various MWs markedly reduce from east to west of the sill so that the numerical values given hereafter are

the extrema expected in the western Alboran. Some MWs are structured like veins and these extrema are those associated with their cores. Therefore, they cannot be specified accurately either with hydrographic sections, even when performed with a sampling interval as small as 2–3 nm, or with time series at fixed locations. They could be accurately specified only with tow–yow devices, which cannot be envisaged in the long-term. Other MWs approaching the sill are already mixed with AW so that actual extrema are markedly depth dependent. Note that, even though the $S_{min}$ associated with NACW can be recognized in most of the sea, it markedly reduces from west to east.

WIW results from AW cooling in the Provençal and the Ligurian (Fig. 2) and can represent relatively large amounts of transformed AW. It was recognized in the strait (Gascard and Richez, 1985) and it is said to occur intermittently in the Alboran (Vargas-Yanez et al., 2002), being characterized by $\theta_{min}$ = 12.9–13.0 °C at 100–300 m. Even though never described in the GE papers, it is clearly indicated on most GE CTD transects east of the sill (see Section 2).

LIW is the most known of all MWs, partly because it is clearly indicated on $\theta$ and $S$ profiles in most of the sea by relative and absolute maxima, respectively, hence forming a bump on a $\theta$–$S$ diagram. However, it is generally forgotten that, along its route from the Levantine to Gibraltar, LIW is involved in the formation of dense MWs in the Aegean, the Adriatic and the Provençal. Therefore, in addition to its own variability in both amount and characteristics when formed, and to its more or less continuous mixing with surrounding MWs all along its route, a specific variability is imposed by these wintertime events. In the end, the variability is so complex that any type of seasonality can hardly be observed at Gibraltar. In the Alboran, $\theta_{max}$ = 13.1–13.2 °C (200–400 m) and $S_{max}$ = 38.50–38.52 (300–500 m). Since the waters above (WIW) and below (TDW) LIW have rarely, if not never, been considered, and as mixing prevents to any separation between them, all these MWs were considered as being LIW, which led assuming that LIW represents up to 90% of the outflow.

TDW results from the mixing of the eastern basin deep MWs (EMDW, by analogy with WMDW) with the MWs resident in the Tyrrhenian. In the Channel of Sicily (sills at 400 m, north–south oriented), EMDW is differentiated from LIW mainly by lower $\theta$ (14.0 vs. 14.5 °C), the EMDW (respectively LIW) core being along the Tunisian/western (respectively Sicilian/eastern) slope. Unmixed EMDW is denser than WMDW (29.15 vs. 29.10 kg m$^{-3}$). When Sparnocchia et al. (1999) reported the cascading of the eastern basin outflow down to ~2000 m, we commented on the regulation of the WMDW amount such a cascading (of only EMDW) would lead to. If the WMDW amount is relatively low, only the WMDW uppermost part will mix with EMDW and TDW will be mainly of eastern origin, its upper part circulating like LIW. If the WMDW amount is relatively large, more of it will mix with EMDW and TDW will be more of western origin, its lower part behaving like WMDW. Obviously, such a WMDW regulation and the TDW characteristics also depend on the EMDW amount and on the fact that not only WMDW but also old LIW and old TDW (see Section 1.2.2) can be found at 400–2000 m in the Tyrrhenian. The relatively large $\sigma$ of the MWs resident there, compared to that of the cascading EMDW, leads to a TDW outflow much thicker than the outflow from Gibraltar that is about twice as large. TDW lies in between the well-known LIW and WMDW and more or less mixes with them, while, on a $\theta$–$S$ diagram, it is located not far from a LIW–WMDW mixing line, which partly explains why it is currently ignored. TDW does not have a well-defined core in the ranges $\theta$ = 13.0–13.1 °C and $S$ = 38.48–38.51. We differentiate hereafter, for convenience, a lower-TDW from an upper-TDW that will behave more like WMDW and LIW, respectively, but TDW has nothing to do with LIW.

The fact that the cool (12.9–13.0 °C) and relatively fresh (38.44–38.48) WMDW, formed by deep convection mainly in the Provençal (~2000 m), can be the densest of the MWs in the western basin has consequences for the outflow that have not been emphasized enough. Indeed (see details in Section 1.2.2), first note that WMDW formed during a specific winter can be more or less dense. The densest WMDW cascades over the bottom at depths >2000 m only, circulates counterclockwise along the continental slope, and is first trapped in the Algerian and the Tyrrhenian before being uplifted more and more by newly formed denser WMDW. The less dense WMDW never reaches depths of 2000 m, mixing and spreading there without circulating significantly. In most of the Alboran (<1500 m), the WMDW specificity is thus that it does not circulate significantly and is markedly mixed, although possibly relatively young or very old. The linear trends (+0.03 °C/decade and +0.01/decade over four decades) in the deeper part of the Provençal (Béthoux et al., 1990) cannot be specified in the study area (Millot et al., 2006).

### 1.2.2. The circulation of the waters

Fig. 2 schematizes, for the western basin and in only one diagram, the set of three diagrams we previously proposed for the circulation of AW and the major MWs in the whole sea. Basically, AW and the MWs circulate as density currents according to processes that are exactly those currently admitted for the cascading and circulation of the Mediterranean outflow northward, due to rotation. Within such a relatively closed basin, all waters thus circulate initially as veins (continuous lines in Fig. 2), alongslope and counterclockwise. Peculiarities about the driving forces and equilibrium levels are: (i) AW flows into the sea to compensate for its water deficit, hence for the sea level difference between the sea and the ocean, (ii) WIW and WMDW formed in the north of the basin are first amassed locally in late winter, above LIW for WIW or on the bottom for WMDW, before spreading all year long, (iii) LIW continues its route from the Levantine without being disturbed by its passage through the Channel of Sicily, (iv) EMDW cascades from this channel and leads to TDW. Note that only the upper-TDW is identified in Fig. 2 while the lower-TDW is not differentiated from the relatively motionless WMDW upper part (see below). Within most of the basin, we thus consider a set of intermediate MWs (WIW + LIW + upper-TDW) and a set of deep ones (lower-TDW + WMDW). Also note (i) the non-occurrence along the African slope of any intermediate vein, (ii) that intermediate MWs entrained in the Algerian interior mix there until no longer associated with any horizontal density gradient, hence no longer circulating and forming old LIW and old TDW somehow trapped in the basin and possibly entering the Tyrrhenian to be involved in the formation of new TDW.

When newly formed WMDW is dense enough to reach the bottom in the Provençal (~2000 m), it amasses there before spreading and circulating at greater depths that correspond to its equilibrium level. Such a WMDW surrounds the Balearic Islands (the channel is 800 m deep) and skips most of the Alboran (depths <1500 m). Since the Channel of Sardinia is only 2000 m deep, WMDW circles in the Algerian (2900 m) where huge yearly means of ~10 cm s$^{-1}$ were measured at ~2700 m off Algeria (Millot and Taupier-Letage, 2005b). This young WMDW is thus trapped there and it uplifts the older but still relatively dense WMDW. Only the part of this older WMDW lifted above 2000 m can outflow into the Tyrrhenian (3500 m), where it will circulate, mix and be trapped as long as not uplifted by denser WMDW. In the Provençal, when newly formed WMDW is not dense enough to reach the bottom, it sinks in a continuously stratified layer of old WMDW and mixes locally at depths <2000 m, hence not circulating.

WMDW (and lower-TDW) found at depths much shallower than 2000 m (i.e. <1500 m) thus does not circulate significantly,

be it newly formed in the Provençal, uplifted in the Algerian and the Tyrrhenian, or markedly mixed anywhere. Due to the Coriolis effect, both the intermediate MWs and AW that circulate alongslope depress the motionless deep MWs by several 100s m in both the north and the south of the Alboran so that, when intermediate MWs do not spread far to the south, the deep MWs can reach shallow levels in between. Since WMDW is formed nearly every winter, it has to outflow from the sea so that it must proceed towards the strait and up to its sill depth. One reason leading to such a westward and upward motion that has never been envisaged up to now could be the WMDW permanent occurrence up to very shallow depths (<100 m) in the Provençal, which could lead to WMDW pressed upward everywhere else. Whatever the case, in the Alboran, (i) WMDW cannot be structured as a vein, so that its average westward speed is necessary low, (ii) its age and characteristics cannot be specified, (iii) it is more or less mixed, (iv) it is mainly located in the south where the intermediate MWs hardly spread.

Considering that both the "intermediate" and the "deep" sets of MWs outflow at depths <300 m, we have found it more correct to deal thereafter with sets of "light" vs. "dense" MWs.

*1.2.3. Recent results at Gibraltar*

The CIESM Hydro-Changes Programme (ciesm.org/marine/programs/hydrochanges.htm, HCP) initiated in the early 2000s maintains moored CTDs (Sea-Bird SBE37-SMs) in the whole sea. The CTD sensors are flushed before sampling, mainly to prevent sedimentation on the conductivity cell. Adequate nominal accuracies (0.002 °C, 0.0003 S/m), resolution (0.0001 °C, 0.00001 S/m) and stability (0.0024 °C/yr, 0.0036 S/m/yr), as well as a multi-year autonomy (1-h sampling), yield deployment duration limited mainly by the mooring resistance. Among others, two CTDs are operated since January 2003 in the strait (Fig. 1), one at Camarinal Sill South (270 m) the other on the Moroccan shelf (80 m). They were serviced in April 2004, November 2005, March 2007 and October 2008. Calibrations made by the manufacturer before January 2003 and after November 2005 and March 2007 give drifts (in °C/yr and S/m/yr) at both 80 and 270 m much lower than the nominal values. Assuming linear drifts during these 33-month and 16-month periods allowed us to check the time series continuity. The CTDs used from March 2007 to October 2008 are not post-calibrated yet, so that data are not shown hereafter and just commented. Resulting from the short mooring length (10 m) and the GPS accuracy, positions/immersions are easily maintained (as confirmed at the recovery). The data set is thus very reliable.

The 2003–2004 time series from the 270-m CTD and other ones from previous experiments indicate (Millot et al., 2006) that the outflowing MWs have been temporarily warming and becoming more saline since the mid 1990s, being in the early 2000s much warmer (∼0.3 °C) and saltier (∼0.06) than ∼20 years ago. Only LIW and upper-TDW, i.e. light MWs, were found at the sill without any dense MWs. As a probable consequence of the EMT, TDW was more of eastern origin than previously; but even more eastern TDW has been encountered since then (see below). The 80-m CTD, set to monitor the inflow, in fact allows monitoring both the inflow and part of the outflow, due to the large amplitude of the internal tide (Millot, 2007). The inflow shows a marked seasonal variability of $S$ (amplitude ∼0.5, maximum in winter), due to air–sea interactions, and a huge ∼0.05 $yr^{-1}$ interannual salinification during the 2003–2007 period. Examples of the time series recorded at both places are given in both papers and a schematic diagram of the MWs distribution at the sill is proposed in Millot et al. (2006).

We already looked for comparisons with more standard hydrographic data and considered the very valuable GE transects. Even though the LYNCH campaign only focused on the strait itself, it is interesting since transects were repeated several times within two weeks from 5°15′W to 6°05′W that were assumed to be the strait entrance and outlet for the MWs. In addition, marked changes occurred during the campaign in the composition of both the set of MWs east of the sill and AW (NACW vs. SAW). Due to mixing, the outflow overall characteristics west of the sill depend less on the composition of the set of MWs than on that of AW (Millot, 2008).

The marked differences between the current thoughts and our personal ones led us to reconsider the former, and we deal hereafter with a "MWs outflow" (not MW outflow) to emphasize its expected heterogeneity. We describe the outflow characteristics first with a re-analysis of GE CTD profiles (mainly GIB1 and GIB2, Section 2) and then with an analysis of the full HCP CTD time series (Section 3). We discuss both analyses in Section 4 before concluding in Section 5.

## 2. A re-analysis of Gibraltar experiment data

A series of north–south CTD transects across the Alboran subbasin, the Strait of Gibraltar and the Gulf of Cadiz were repeated several times during several GE campaigns in1985–1986 (Fig. 1). The LYNCH-702-86 (November 1985), GIB1 (March–April 1986) and GIB2 (September–October 1986) data available in the MEDATLAS database (MEDAR group, 2002) are of particular interest and we analyzed all the profiles available between 4°30′W and 6°15′W. The interest of the LYNCH data was already specified (in Section 1.2.3) and some data are shown hereafter. The GIB1 and GIB2 data are interesting because, even though transects were not repeated, they covered the whole study area within one week. The features indicated in the GIB1 and GIB2 transects suggest relatively stable dynamical regimes during both campaigns, making them suitable for a description of the outflow, and significant differences between them illustrate some aspects of the variability. We thus

**Table 1**
Beginning time of the GIB1 and GIB2 CTD profiles. Also specified are the dates of the first and last profiles for each transect, as well as the profile color (see text).

| GIB1 | | GIB2 | |
|---|---|---|---|
| 6°15′ | 2/04/86 05:19<br>06:39,07:49<br>2/04/06 09:01 | 6°05′ | 26/09/86 17:21<br>18:29,19:06,19:42<br>26/09/86 20:22 |
| 5°15′ | 12/04/86 13:32<br>14:07,14:52,16:00,17:08,<br>18:29,19:56,<br>20:53, 12/04/06 21:45 | 6°15′ | 27/09/86 02:37<br>03:57,04:35,05:10,06:00,<br>06:41,07:43<br>27/09/86 08:30 |
| 5°00′ | 12/04/86 23:51<br>00:36,02:07,03:54,05:40,07:20<br>13:04:86 08:41 | 5°50′ | 29/09/86 00:28<br>01:02,01:42,02:26,03:27,04:13<br>29/09/86 04:44 |
| 4°30′ | 13/04/86 13:44<br>15:40,17:10,19:38,22:<br>36,00:57,03:02,<br>05:05, 14/04/86 05:40 | 5°40′ | 29/09/86 07:32<br>08:09,09:09,09:58,11:07<br>29/09/86 12:00 |
| 5°30′ | 16/04/86 17:20<br>17:57,19:04,20:12<br>16/04/86 22:33 | 5°30′ | 29/09/86 15:04<br>16:02,17:06,18:00<br>29/09/86 19:20 |
| 5°40′ | 17/04/86 00:16<br>00:55,01:33,02:24,03:17<br><br>17/04/86 04:07 | 5°15′ | 29/09/86 21:57<br>22:47,23:29,01:07,02:16,<br>03:28,04:35,<br>05:34,06:30, 30/09/86 07:20 |
| 5°50′ | 18/04/86 20:56<br>22:02,22:47,23:32,00:25,<br>01:08<br>19/04/86 02:01 | 5°00′ | 30/09/86 10:56<br>12:11,13:35,15:05,16:50,18:21<br>30/09/86 19:27 |
| 6°05′ | 19/04/86 11:52<br>12:30,13:00,13:38<br><br>19/04/86 14:17 | 4°30′ | 03/10/86 21:21<br>22:24,00:17,02:21,05:36,<br>08:00,09:43<br>04/10/86 10:24 |

present hereafter mainly the GIB1 and GIB2 data (Fig. 1, Table 1). More accurate locations can be found in the literature. Dates and times in Table 1 define the profiles we considered.

The GIB1 and GIB2 transects are all of great value since they were performed with relatively small sampling intervals, ranging from ~2 nm (sometimes less) in the strait to ~3 nm outside of it, generally down to a few metres above the bottom, and as rapidly as possible. The longest deepest transects (4°30′W, 5°00′W, 5°15′W) were completed in 10–15 h and the shortest shallowest ones (5°30′W, 5°40′W, 5°50′W, 6°05′W, 6°15′W) in 4–6 h. These eight transects were not always performed successively, which led to overall surveys lasting about a week while the required minimum is about four days. As done by all previous authors, we consider that these transects are representative of a synoptic situation and do not depend on the relatively important tidal mixing variability with time. As usually, we thus consider only the mixing variability with space.

When analyzing hydrographic transects so different in both north–south extent (4–70 nm) and maximum depth (300–1400 m) with figures drawn with different $y$–$z$ scales and focusing on the locations where data are available, one must keep in mind the areas these transects actually represent as well as the consequences for both the MWs outflow and the AW inflow. For instance (Fig. 3), the transports of both the outflow and the inflow through the 4°30′W section (90 nm, 1400 m) being similar to those through the sill/5°45′W section (20 nm, 300 m), which has an area about 30 times less, the distribution and speed of both flows markedly vary from one section to the other. Fig. 3 also allows an overview of the GIB1 and GIB2 data. East of the sill, the $\sigma$ = 28.75 kg m$^{-3}$ isoline is assumed to represent the AW–MWs interface while, as argued later on, separation of the light and dense MWs can be done with $\sigma$ = 29.08 kg m$^{-3}$; west of the sill, other representative values were chosen. Fig. 3 helps understand the difficulty of the sampling since ship drifts during a CTD profile can be relatively important due to large currents, not considering navigational constraints and commercial traffic. Even though the bathymetry can be relatively steep, the fact that most of the profiles were made down to a few metres above the bottom helps ensure that, in general, no significant amount of the MWs was missed. Figures are drawn using all data available in the MEDATLAS database with pressure intervals of 2 dbar for GIB and 1 dbar for LYNCH.

Data are analyzed from west to east and for GIB1 and GIB2 simultaneously, first with $\theta$–$S$ diagrams, then with $y$–$z$ sections for $\theta$, $S$ and $\sigma$. The $\theta$–$S$ diagrams for all sections between 4°30′W and 5°50′W are drawn with the same scales and with acronyms specified at exactly the same positions to facilitate profiles comparisons. Those from 5°50′W to 6°15′W are drawn with extended scales to represent more data. Profiles that clearly indicate in their upper part the WIW and/or LIW cores, hence light MWs, are plotted in red. Those indicating dense MWs only are plotted in blue while the ones indicative of both light and dense MWs are plotted in violet. As expected (Section 1.2), a general result will be that red profiles are in the north, blue profiles in the south and violet profiles in between. To simplify the analyses, the correspondence between the shape of the profiles (i.e. the MWs they evidence) and their location (in a north–south direction) is not emphasized. Also, the measured extrema, in particular those associated with the light MWs, do not regularly reduce westward up to the sill, which is due to a still too large sampling interval for MWs structured as veins, not considering their own heterogeneity.

### 2.1. The 4°30′W data

The $\theta$–$S$ diagrams in Fig. 4 indicate all four major MWs during both GIB1 and GIB2. WIW was more clearly noticed during GIB2 (12.9–13.0 °C, 38.25–38.35) than during GIB1 (~13.05 °C, ~38.25) while LIW was less mixed during GIB1 (13.05–13.10 °C, 38.45–38.47) than during GIB2 (~13.05 °C, ~38.45). Several GIB1 and two GIB2 red profiles indicate low WIW amount, hence a direct AW–LIW mixing. The deepest among the red profiles also indicate, below LIW, both TDW and WMDW. Note that TDW is indicated by the curved shape of the diagrams between LIW and WMDW, which cannot result from a mixing between only LIW and WMDW.

During GIB1 (Fig. 4a), two violet profiles only indicate lower-TDW (not WMDW) in their deeper part, then heterogeneities clearly resulting mainly from LIW (not WIW), and finally mixing with AW. During GIB2 (Fig. 4b), no violet profiles were observed. Instead, one relatively smooth blue profile tends to directly link AW and WMDW, with some bending due to lower-TDW, thus clearly showing that dense MWs mix with AW far away from the sill, in the south and to depths of ~400 m at least (see Fig. 5). The orange and brown plots allow estimating the GIB1–

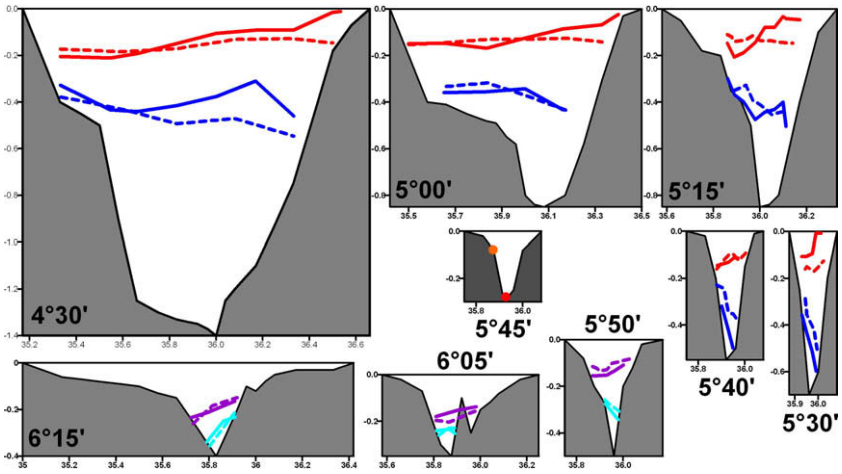


**Fig. 3.** North–south bathymetric sections inferred from a navigation chart with a 5 nm interval aimed at comparing the transects areas, hence plotted with similar $y$-latitude (in tens of degrees) and $z$-depth (in km) scales. Specific bathymetric features, such as Camarinal Sill centered at ~5°45′W but orientated NNW-SSE, are roughly represented, and some transects are not exactly north–south or straight. Isopycnals $\sigma_{LD}$ = 29.08 kg m$^{-3}$ and $\sigma_{AM}$ = 28.75 kg m$^{-3}$ are in blue and red, respectively, for GIB1 (full) and GIB2 (dashed) east of the sill; west of it, $\sigma_{AM}$ = 27.0 kg m$^{-3}$ (violet) while $\sigma_{LD}$ = 29.0, 28.5 and 28.0 kg m$^{-3}$ (cyan) at 5°50′W, 6°05′W and 6°15′W, respectively. Isopycnal coloring is reproduced in sections thereafter. The red and orange dots (5°45′W) represent the CTD sites at 270 and 80 m. (For interpretation of the references to color in this figure legend, the reader is referred to the web version of this article.)

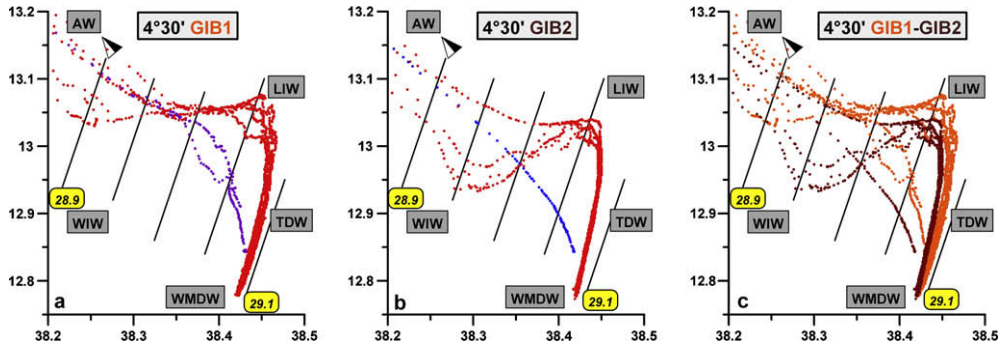


**Fig. 4.** $\theta$–$S$ diagrams for the 4°30′W transect: GIB1 (a), GIB2 (b), both (c). Till 5°50′W, the $\theta$ and $S$ scales are the same and arbitrarily fixed acronyms (see text) are still at the same place. In both (a) and (b), the red profiles indicate the WIW and/or LIW cores, the violet profiles indicate marked influence of the WIW and/or LIW veins while the blue profiles indicate a direct mixing between AW and either lower-TDW or WMDW (no influence of either WIW or LIW). In (c), the GIB1 (respectively GIB2) profiles are orange (respectively brown). Isopycnals are plotted 0.05 kg m$^{-3}$ apart. (For interpretation of the references to colour in this figure legend, the reader is referred to the web version of this article.)

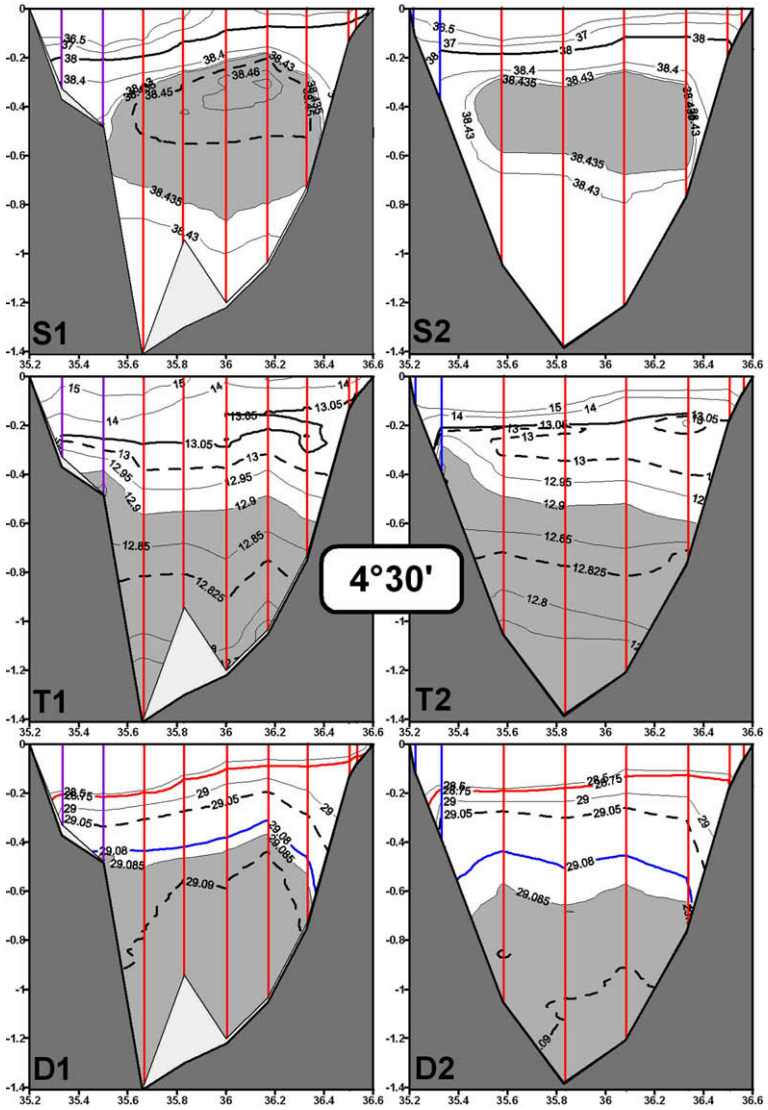


**Fig. 5.** The 4°30′W GIB1 and GIB2 transects in salinity (S1 and S2), potential temperature (T1 and T2) and potential density anomaly (D1 and D2). Profiles are colored as explained in Fig. 4 and indicated in Table 1. For S1 and S2, $S$ = 38.00 is thick, $S$ = 38.45 is dashed, $S$ > 38.435 are in grey. For T1 and T2, $\theta$ = 13.05 °C is thick, $\theta$ = 12.825 °C and $\theta$ = 13.00 °C are dashed, $\theta$ < 12.90 °C are in grey. For D1 and D2, $\sigma$ = 28.75 kg m$^{-3}$ is red, $\sigma$ = 29.08 kg m$^{-3}$ is blue (as in Fig. 3), $\sigma$ = 29.05 kg m$^{-3}$ and $\sigma$ = 29.09 kg m$^{-3}$ are dashed (see Section 4.4) and $\sigma$ > 29.085 kg m$^{-3}$ are in grey. Most profiles were down to (thin line and light grey area) a few metres above the bottom (thick line and dark grey area); in general, the maximum-depth and bottom-depth lines cannot be differentiated on the figures. The northern and southern limits of the transect (depth = 0) are not realistic (see Fig. 3) and were arbitrarily fixed not too far the nearest profile, but information there is not reliable. Most of these values and comments apply till 6°15′W. (For interpretation of the references to colour in this figure legend, the reader is referred to the web version of this article.)

GIB2 differences (Fig. 4c; references to $\theta$–$S$ diagrams a, b, c are, in general, not specified hereafter). Both LIW and TDW were more mixed during GIB2 than during GIB1, even though roughly the same WMDW was sampled at the densest levels. Note that $\sigma = 29.08$ kg m$^{-3}$ can be used to separate, for the red and violet profiles, an upper irregular part associated with the light MWs from a lower smooth part associated with the dense MWs (this will be possible up to the sill).

The sections (Fig. 5) show that the northernmost profiles only indicate WIW. The WIW $\theta_{min}$ is at 150–200 m (GIB1) and ~200 m (GIB2) while LIW is more clearly indicated by its $S_{max}$ at ~300 m (GIB1) and 400–500 m (GIB2) than by its $\theta_{max}$ at ~200 m (GIB1) and ~300 m (GIB2). The WIW core is close to the upper slope, so that red profiles indicating mixed WIW are more to the south. Even though the LIW core (actually between $\theta_{max}$ and $S_{max}$) is also close to the northern slope, the LIW influence can reach the whole southern slope (GIB1) or only part of it (GIB2). As usual, TDW is never clearly indicated while WMDW is clearly indicated by its low $\theta$, relatively low $S$ and high $\sigma$. Below 500 m and at given depths, the TDW $S$ and $\theta$ values were higher during GIB1 than dur-

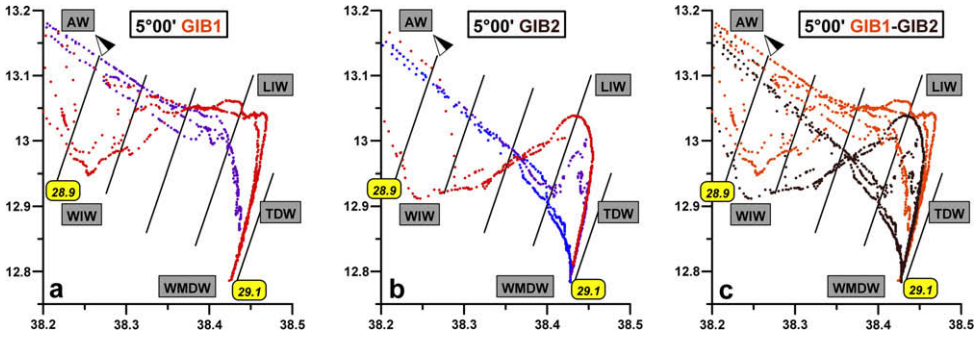


**Fig. 6.** As in Fig. 4 for 5°00′W.

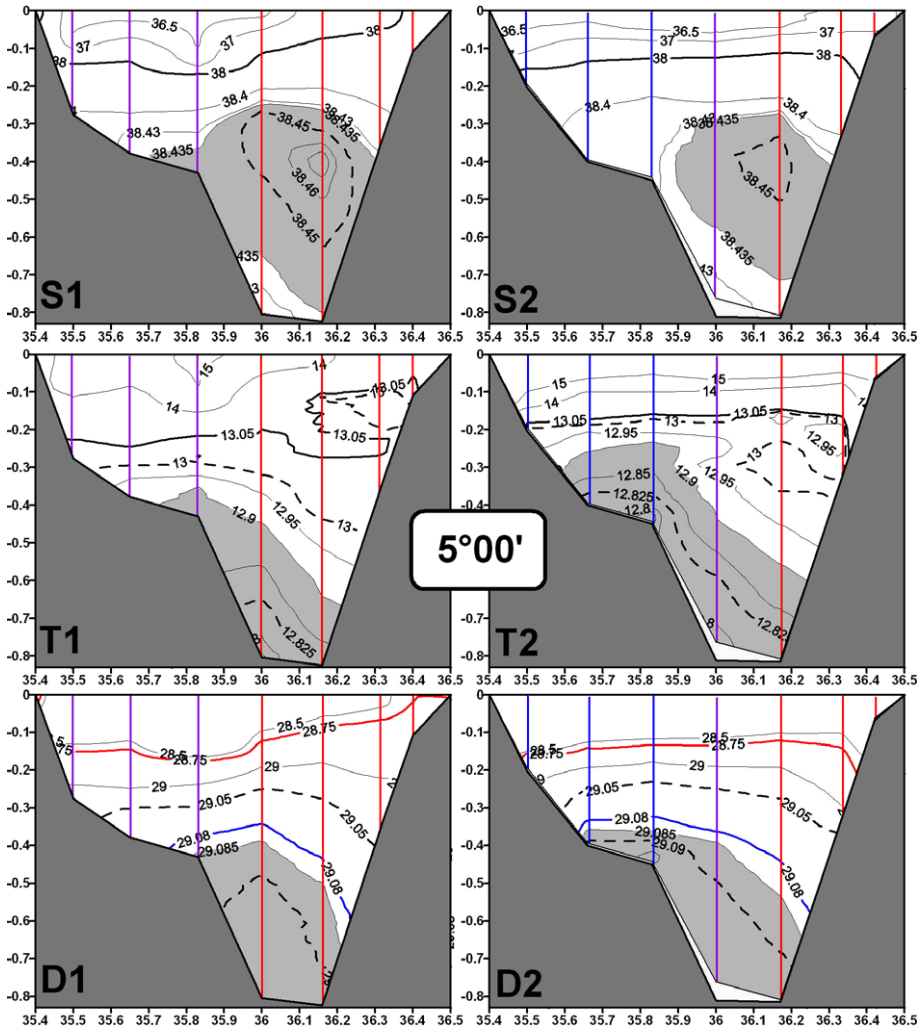


**Fig. 7.** As in Fig. 5 for 5°00′W.

ing GIB2. Even though $\sigma$ was higher too, there was more TDW (vs. WMDW) during GIB1 than during GIB2. Also considering the relative amounts of WIW vs. LIW allows concluding that both light and dense MWs were more from the eastern basin during GIB1 and more from the western basin during GIB2.

### 2.2. The 5°00′W data

The shallowest GIB1 and GIB2 red profiles (Fig. 6) indicate that WIW is more mixed during GIB1, and some GIB1 (no GIB2) profiles only indicate little of it. General features for LIW are re-

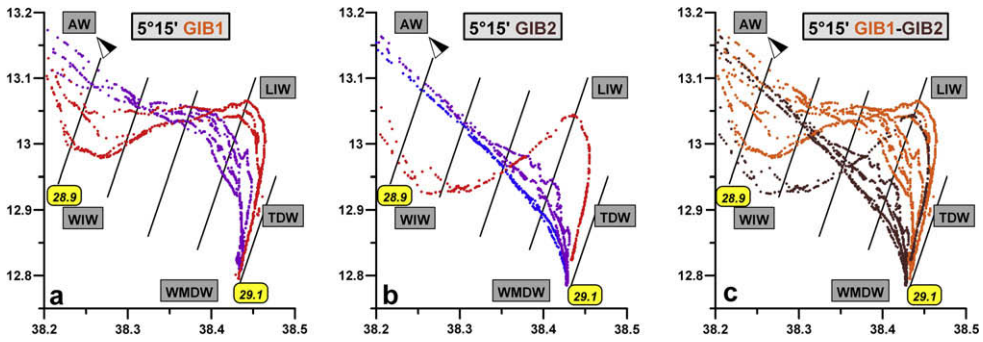


**Fig. 8.** As in Fig. 4 for 5°15′W.

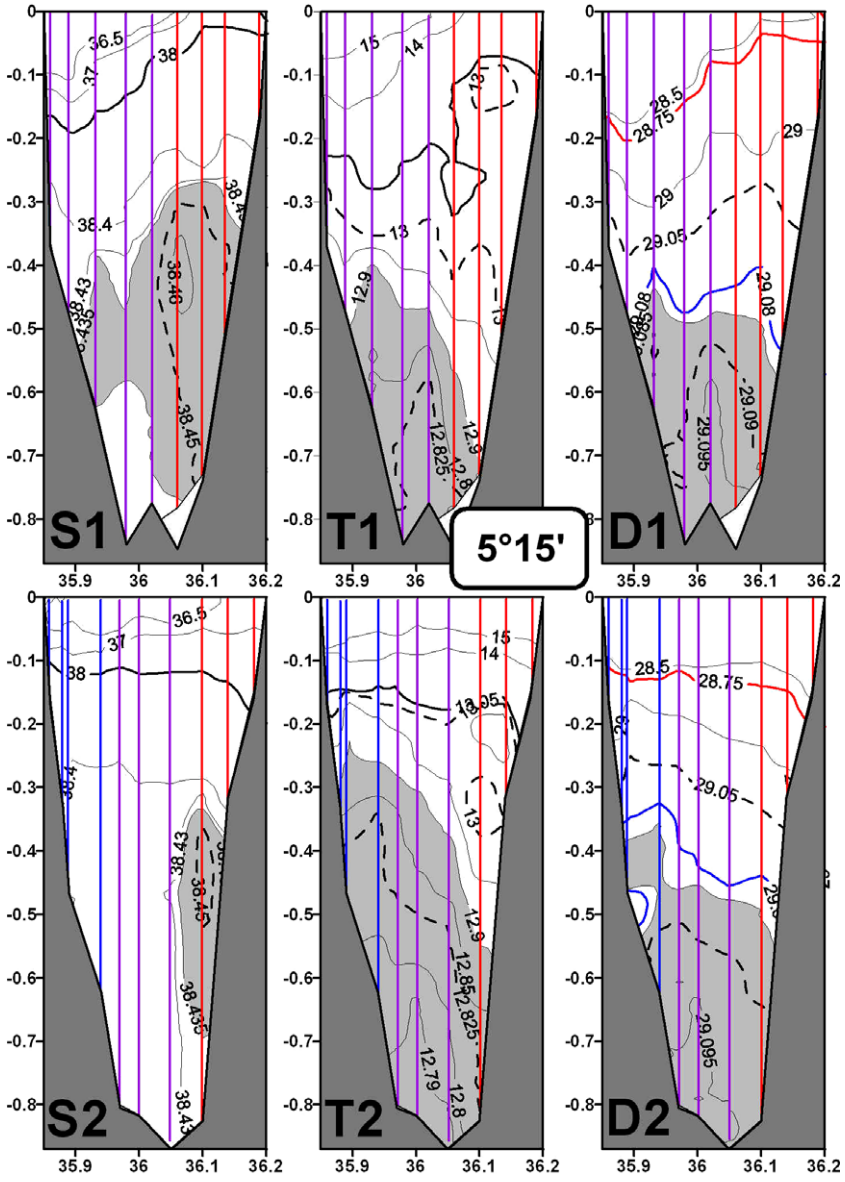


**Fig. 9.** As in Fig. 5 for 5°15′W.

versed, with LIW more mixed during GIB2. However, similar numbers of data representative of WIW and LIW during GIB1 and GIB2 indicate similar amounts. All other GIB1 profiles were violet while only one violet profile was observed during GIB2 together with three blue ones. Note that $\sigma > 29.09\ kg\ m^{-3}$ was found during GIB2 with some red, violet and blue profiles, but the largest values were blue even though the blue profiles were not the deepest ones (Fig. 7). *S* sections essentially show the LIW core at ~400 m during GIB1 and GIB2 but the GIB1 LIW amount is larger than the GIB2 one. $\theta$ sections show the WIW

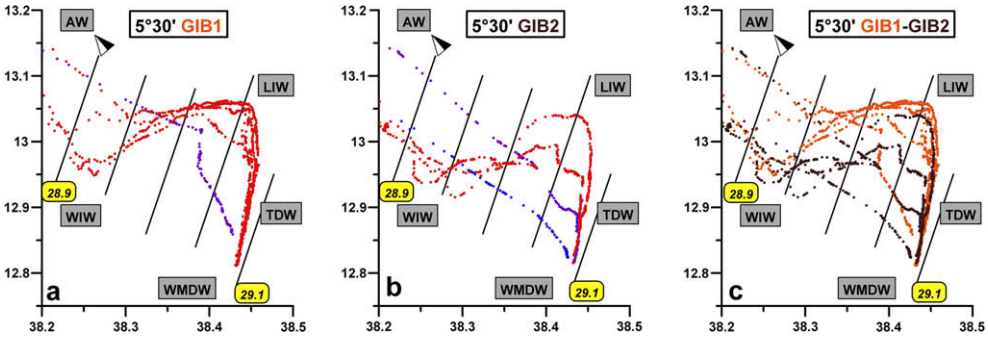


**Fig. 10.** As in Fig. 4 for 5°30′W.

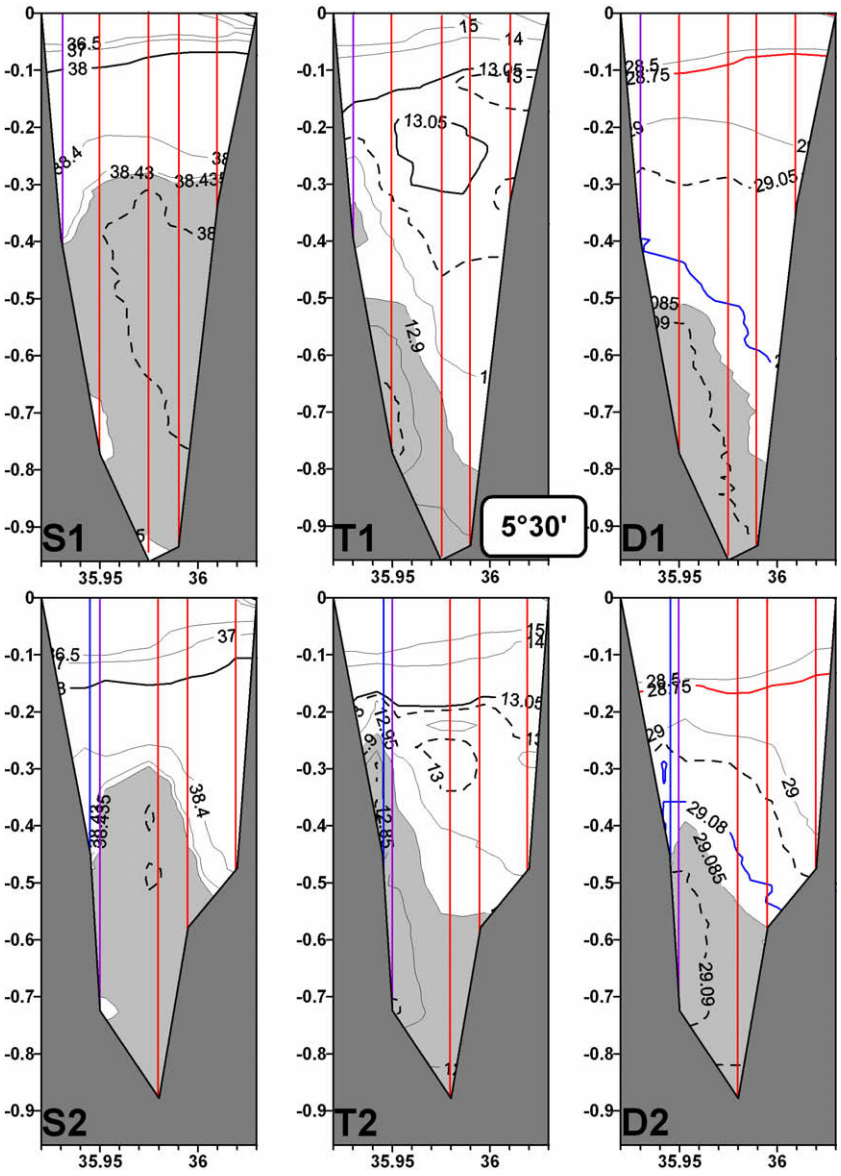


**Fig. 11.** As in Fig. 5 for 5°30′W.

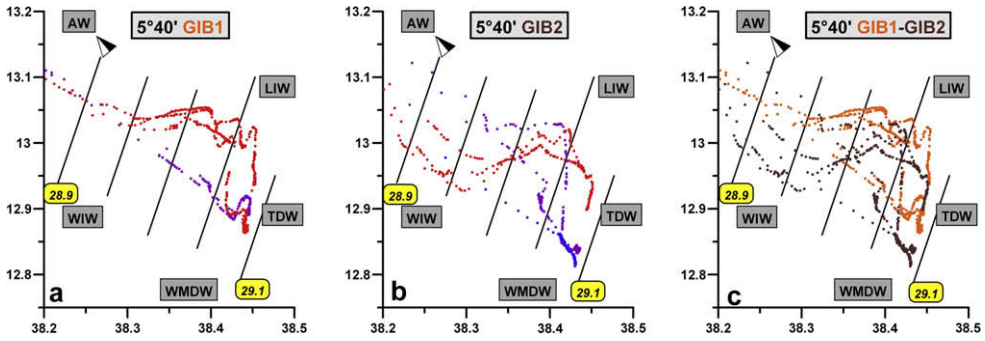


**Fig. 12.** As in Fig. 4 for 5°40′W.

core at 100–200 m (GIB1) and 200–250 m (GIB2), together with the LIW core at 200–250 m (GIB1) and ~300 m (GIB2). In the deeper part of the transects, the WMDW $\theta_{min}$ are relatively similar during GIB1 and GIB2 but they spread more southward up to 400–500 m during GIB2. Consistently, largest GIB2 $\sigma$ also spread more southward so that deepest isopycnals start tilting up southward. Direct mixing between the dense MWs and AW is indicated down to ~400 m (maximum depths) over nearly all the southern half of the GIB2 transect.

### 2.3. The 5°15′W data

Since characteristics indicated by the red, violet and blue profiles at 5°15′W (Fig. 8) are not very different from those at 4°30′W (Fig. 4) and 5°00′W (Fig. 6), the MWs mixing does not markedly intensify along their westward route in the Alboran. The WIW amount is comparable (GIB1) or even larger (GIB2) than the LIW one. The *S* sections (Fig. 9) show more abundant and less mixed LIW during GIB1, cores having deepened to 400–500 m (deeper by 50–100 m than at 5°00′W) during both GIB1 and GIB2. $\theta$ sections still show the WIW core at 100–200 m (GIB1) and 200–250 m (GIB2), and the LIW core at 250–300 m (GIB1) and 300–350 m (GIB2), hence ~50 m deeper than at 5°00′W. Lowest $\theta$ and highest $\sigma$ indicate that the densest MWs are found in the deeper part of the transect and tend to spread over the southern slope. Mixing of the dense MWs directly with AW is observed in the south down to ~600 m.

### 2.4. The 5°30′W data

The red profiles in Fig. 10 indicate WIW and LIW extrema as large, and even sometimes more pronounced, than at 4°30′W, confirming the reduced mixing of the light MWs downstream and the veins heterogeneity. The WIW amount is still comparable (GIB1) or even larger (GIB2) than the LIW one. The major differences with the profiles more to the east come from the violet and blue ones during GIB2 that tend to become AW–TDW and AW–WMDW mixing lines, respectively, which will appear to be a significant tendency. The very different shapes of nearby profiles, such as the two deepest red ones as well as the violet and the blue ones during GIB2, illustrate the difficulty of correctly sampling not only the light MWs cores but also the dense MWs. During GIB2, roughly the same dense MW sampled in the deepest parts of the red (at ~900 m; Fig. 11), violet (at ~700 m) and blue (at ~400 m) profiles spread over the deepest part of the southern slope. However, only its shallower/southernmost part (the blue profile) mixed with AW; note that the AW–TDW mixing at the nearby location (the violet profile) also reaches a maximum depth close to 400 m.

The LIW *S* core there is less clearly noticeable than more to the east, and it has markedly deepened along the slope during

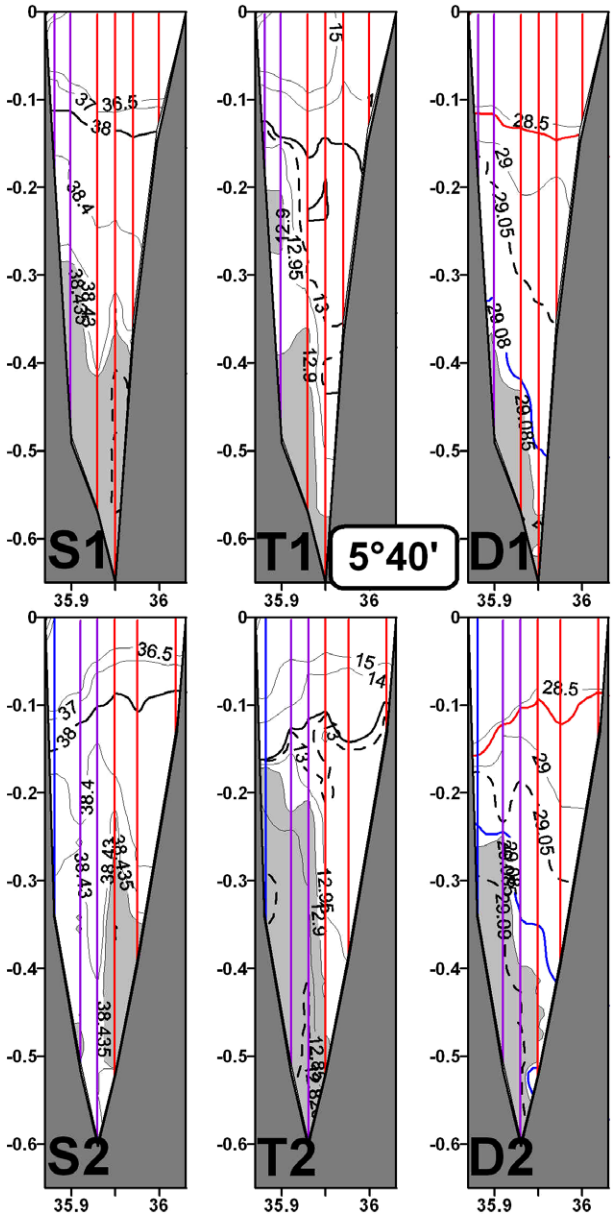


**Fig. 13.** As in Fig. 5 for 5°40′W.

GIB1 while it has moved toward the strait central part during GIB2 (Fig. 11). $\theta$ sections still show the WIW core at 100–200 m (GIB1) and as deep as ~300 m (GIB2); they show the

LIW core at 200–300 m (GIB1) and ~300 m (GIB2). Associating both the extrema amplitude and the relative areas occupied by WIW and LIW with the relative amounts of the two waters, the GIB1 and GIB2 data clearly illustrate an interaction between them along their westward route. During GIB1, the WIW amount is relatively low but WIW does not encounter major changes while the LIW amount is relatively large and LIW deepens, probably due to increasing velocities. During GIB2, the WIW amount is relatively large and WIW deepens while the LIW is relatively low and LIW is found away from the slope. Clearly, the larger the light MW amount, the larger its westward velocity and its tendency to deepen, due to rotation, and to push away the MW below, but not modifying markedly the MW above. During GIB1 and GIB2, lowest $\theta$ and highest $\sigma$ occur in the south of this V-shaped passage where deep isolines tend to parallel the slope.

### 2.5. The 5°40′W data

Approaching the sill (just ~5 nm to the west), mixing intensifies markedly and leads to a relatively complex situation (Fig. 12). During GIB1, little amount of WIW is indicated on the available profiles down to ~100 m. Considering the amount and immersion of the WIW core more to the east, it might be that most WIW outflows more to the north. The four (out of six) red profiles show an AW–LIW mixing line while below, the LIW vein encounters marked disturbances. During GIB2, three (out of six) red profiles indicate that the WIW amount is still relatively large and that WIW $\theta_{min}$ are still in the 12.90–12.95 °C range, so that WIW can clearly be an important component of the MWs outflow. During GIB1, two violet profiles were straighter than previously, indicating an intensified AW–TDW mixing. During GIB2, none of the two violet profiles was as straight as at 5°30′W while no violet profiles similar to the 5°40′W ones were observed at 5°30′W. A similar remark concerns the blue GIB2 profile that is not as straight as (or straighter than) at 5°30′W; differentiating it from the violet profiles was maintained as regard to continuity between the 5°30′W and 5°50′W data. The $S$ distribution (Fig. 13) shows during GIB1 an LIW core still at 400–600 m, thus close to the deeper part of the strait there, and still along the slope while $S$ values during GIB2 are much lower and the core is still pushed away from the slope. The $\theta$ distribution during GIB2 indicates a large data amount in the 12.95–13.00 °C range at 200–300 m close to the northern slope, so that WIW actually represented a significant part of the outflow. The LIW $\theta_{max}$ is more marked during GIB1. The lowest $\theta$ values, associated with the largest $\sigma$ values, along the southern slope indicate both lower-TDW and WMDW, the latter during GIB2 only.

### 2.6. The 5°50′W data

Homogeneity of all profiles has increased, as expected 5 nm west of the sill, but marked north–south differences are still indicated. To emphasize the continuity with those more to the east, $\theta$–$S$ diagrams are first shown with the same scales (Fig. 14). Because the diagrams there are mainly mixing lines between some MW and AW, they were no longer colored according to their shape but according to the MW expected to be involved. Profiles involving either WIW or LIW are red while those involving TDW and WMDW are violet and blue, respectively. We also found more interesting to display in 14c the LYNCH data instead of the GIB1–GIB2 comparison, all being compared later on. LYNCH transects were performed twice, on both November 3 (LYNCH12) and 14 (LYNCH34), at locations roughly similar to the #1 (south) to #5 (north) GIB1 and GIB2 ones but the dramatic changes that occurred during the campaign prevent from a priori coloring the profiles.

Among the seven GIB1 profiles (Fig. 14a), the most straight and most southward one in the red group (#3) represents only AW–LIW mixing ($\sigma_{max} \sim 29.01$ kg m$^{-3}$) and does not indicate any WIW. Other ones, in particular the northernmost #6–7, indicate AW–WIW mixing only. The WIW signature on #4–5 accounts for the WIW importance even when in relatively low amount. The violet group (2 relatively close profiles, $\sigma_{max} \sim 29.03$ kg m$^{-3}$) indicates a similar AW–TDW mixing with few points near the #6–7 lower part. Even though the AW–WIW and AW–TDW mixing lines are partly superimposed, it is clear that the outflow is separated into three juxtaposed "suboutflows" that have markedly different $\theta$–$S$ characteristics, maximum depth (see Fig. 17) and north–south location, the densest (respectively lightest) being the southernmost (respectively northernmost one). The $\sigma_{max}$ associated with TDW and LIW differ by only ~0.02 kg m$^{-3}$ and are larger by ~0.1 kg m$^{-3}$ than the WIW one.

During GIB2 (Fig. 14b), which was characterized upstream by relatively large amounts of WIW vs. LIW and WMDW vs. TDW, a WMDW blue group (#1–2, $\sigma_{max} \sim 29.05$ kg m$^{-3}$) that is the southernmost one is differentiated from a TDW violet group (#3–4, $\sigma_{max} \sim 29.025$ kg m$^{-3}$). Profile #5/GIB2 is extremely interesting since it shows a gap (28.911–28.945 kg m$^{-3}$) and can thus be separated in two. Extrema reached by its deeper part are just slightly lower than the #3/GIB1 ones and thus indicate LIW, which is consistent with LIW during GIB2 more mixed than during GIB1. Extrema reached by its lower part correspond to the #6/GIB1 ones, hence accounting for the WIW importance also during GIB2. The GIB2 outflow was thus subdivided into four juxtaposed suboutflows, the interface between the WIW and LIW ones being inclined and intersected by #5 (see comments below about #6/GIB2). The $\sigma_{max}$ associated with WMDW, TDW and LIW differ from each other by only ~0.03 kg m$^{-3}$ and are larger by 0.1–0.15 kg m$^{-3}$ than the WIW one.

The four LYNCH transects (Fig. 14c) illustrate the tremendously large variability that can exist west of the sill just ~10 days apart, mainly due to changes in the nature of AW (see Section 1.2.3). All LYNCH12 green profiles were relatively similar, in terms of rough location and slope, while the LYNCH34 cyan ones can be separated into a southern group (#1–2–3) and a northern one (#3–4–5), #3 belonging to one or the other group a few hours apart.

Comparing all diagrams in Fig. 14 allows two remarks. Within each group, mixing lines can be similar with markedly different $\sigma_{max}$ at markedly different depths (i.e. #1–2/GIB2; comparatively, #1–2/GIB1 reach less different depths). Since profiles nearly reached the bottom, this information demonstrates that the suboutflows are continuously stratified, the actual overall $\sigma_{max}$ occurring at greatest depths. Differences in $\sigma_{max}$ between groups during one campaign or for a group between the two campaigns can thus appear unreliable. However, plotting all diagrams together supports the profiles characterization and grouping we made (Fig. 15a). In particular, note that (i) the WIW (pink) suboutflow is indicated by #6–7–(5)/GIB1 and #5–6/GIB2, (ii) the LIW (red) one by #3–4–(5)/GIB1 and #5/GIB2, (iii) the TDW (violet) one by four indiscernible points (#1–2/GIB1 and #3–4/GIB2), (iv) the WMDW (blue) one by #1–2/GIB2 only. Also note that associated $\sigma_{max}$ increase from north (WIW) to south (WMDW) while the associated $\theta$ decrease, and that the LYNCH grey dots concentrate around or tend toward GIB ones, which could allow coloring them accordingly.

The same $\theta$–$S$ diagrams displayed over extended ranges (Fig. 16A for the MWs, Fig. 16B for AW) provide essential information and allow direct comparisons with the data downstream. First, all profiles in Fig. 16A are mixing lines between some AW and some MW. During GIB1 (Fig. 16Aa), profiles #1–2 (violet) and #3–4 (red) indicate different MWs (TDW vs. LIW) in their densest part and tend towards the same kind of AW while profiles #5–6–7 (red, mainly associated with WIW) tend toward another kind of

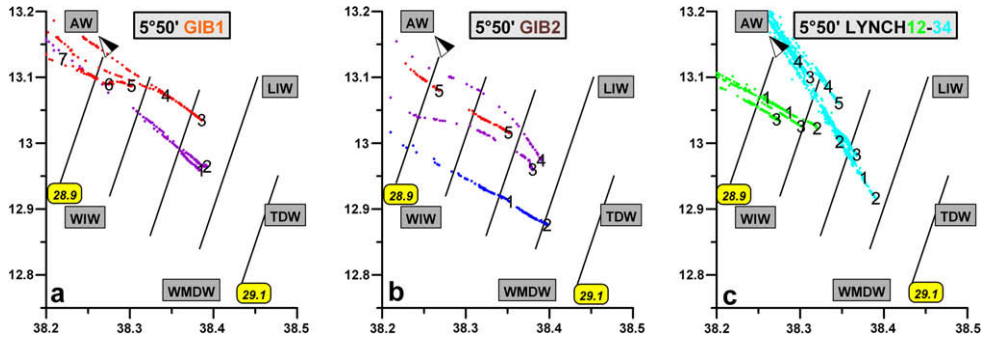


**Fig. 14.** $\theta$–$S$ diagrams at 5°50′W for GIB1 (a), GIB2 (b) and LYNCH (c) with scales as in Fig. 4 (MWs acronyms are no more informative). Profiles numbers (GIB locations in Fig. 17) from south to north are specified at the largest $\sigma$ value. Colors for (a) and (b) are as before (see Fig. 4). Color for (c) is green for transects 1,2 at the beginning (#2 only once) and cyan for transects 3, 4 at the end (∼10 days after, #1 only once). (For interpretation of the references to colour in this figure legend, the reader is referred to the web version of this article.)

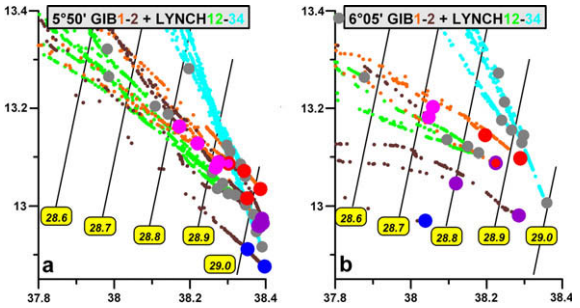


**Fig. 15.** $\theta$–$S$ diagrams at 5°50′W (a, all plots in Fig. 14) and 6°05′W (b, all plots in Fig. 18) in reduced ranges to focus on the $\sigma_{max}$ values specified by dots that are pink (WIW), red (LIW), violet (TDW), blue (WMDW), grey (unspecified, LYNCH)) for GIB1 (orange), GIB2 (brown), LYNCH12 (green) and LYNCH34 (cyan). (For interpretation of the references to colour in this figure legend, the reader is referred to the web version of this article.)

AW. Similarly, during GIB2 (Fig. 16Ab), profile #3 is different from #1–2 in their densest part (WMDW vs. TDW) and becomes similar to them in their less dense part. Profile #6/GIB2 is now indicated and, due to both its similarities with the #5 upper part and its northernmost location, it is red and associated with WIW, which is consistent with the relatively large WIW–GIB2 amount upstream. During LYNCH12, #1–2–3 and #4–5 form clearly different groups and the upper-part profiles tend to spread according to their north–south location. During LYNCH34, the two groups of profiles due to the MWs (#1–2–3 vs. #4–5) tend to form only one group upward. Note the similarities between the two groups of profiles during both GIB1 and GIB2 with either the LYNCH12 or LYNCH34 ones.

Fig. 16B explains the upper-part profiles spreading indicated by Fig. 16A. Both NACW and SAW occurred, the latter displaying seasonal variations between spring (GIB1) and fall (GIB2, LYNCH). However, nearly opposed situations were encountered since dur-

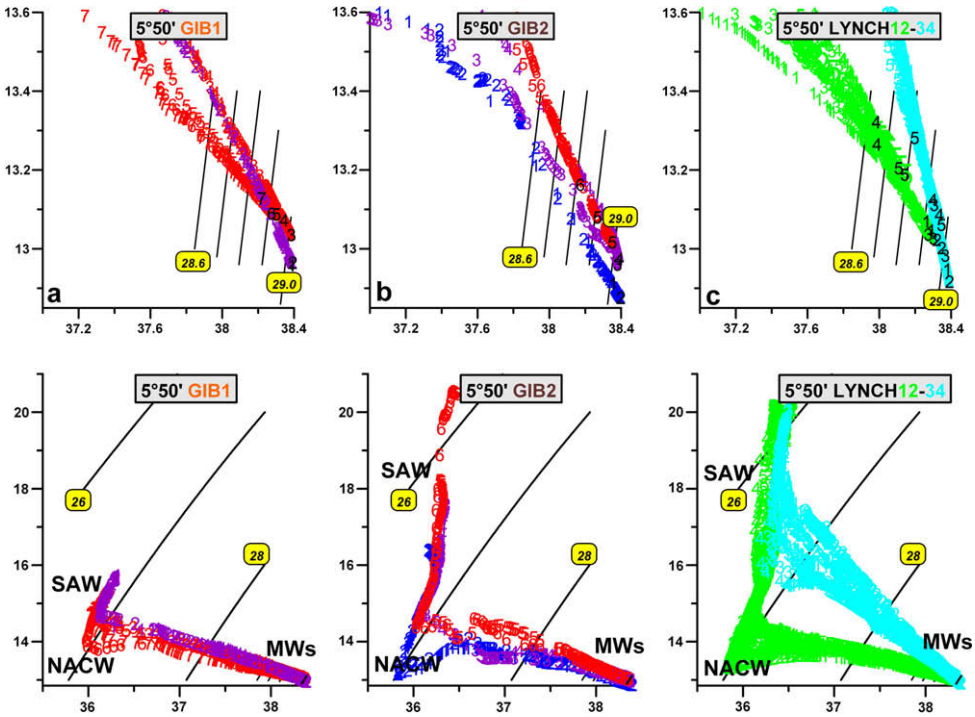


**Fig. 16.** (A) Same as in Fig. 14 but for MWs wider ranges (same till 6°15′W). Additional profiles in the northern part of the GIB1 and GIB2 transects were out of range in Fig. 14. To better differentiate the profiles, dots are replaced by the profile #. Isopycnals are 0.1 kg m$^{-3}$ apart. Profiles #2/LYNCH12 and #1/LYNCH34 were performed only once. (B) Same as in Fig. 16A but for wider ranges to represent both the MWs and AW (NACW and SAW; see definitions in the text). Isopycnals are 1.0 kg m$^{-3}$ apart.

ing GIB1, SAW was mainly in the south (#1–4) and NACW mainly in the north (#5–7) while during GIB2, SAW was mainly in the north (#4–6) and NACW mainly in the south (#1–3). These variations of the NACW vs. SAW distributions in both time and space were observed along the other transects during both GIB1 and GIB2, which guarantees their significance. Even though such spatial variations have never been mentioned and were unexpected, the temporal ones in the long-term (6 months apart for GIB) were less dramatic than the LYNCH ones in the short-term (Fig. 16Bc). During LYNCH, only NACW was present at the beginning (green) while only SAW was present at the end (cyan) ~10 days after. As for GIB1 and GIB2, the LYNCH variations were observed as far as in the eastern Alboran. The marked changes that occurred during LYNCH in the composition of the MWs outflow east of the sill cannot be due to the changes in the distribution of NACW vs. SAW (Millot, 2008). Fig. 16Ac and Bc demonstrate that the whole MWs outflow characteristics dramatically depend on the AW ones in the sill surroundings.

Fig. 17 shows that the two violet GIB1 profiles and the two blue GIB2 ones were roughly at the same place, as were (i) two red GIB1 profiles and the two violet GIB2 ones, (ii) the red #5/GIB1 (mixture of WIW and LIW) and #5/GIB2 (WIW above and LIW below). According to the available data, each of the four major MWs leads to a suboutflow during GIB2 while no suboutflow can be associated with WMDW during GIB1, consistently will all data upstream. The characteristics of the outflow can thus change dramatically at a given location/latitude, depending on the relative amounts of the MWs that, when present, are juxtaposed in the same way from north to south and mix individually with AW. The outflow is subdivided, as soon as 5°50′W, into a series of suboutflows that are associated with the MWs indicated upstream and are located side by side, the densest being the southernmost one. The southernmost profiles indicate the densest MWs along the lower part of the slope during both GIB1 and GIB2 since $\sigma \sim 29.0$ kg m$^{-3}$ (representative of the MWs) tilts up southward while $\sigma \sim 28.0$ kg m$^{-3}$ (the AW–MWs interface there) tilts up northward.

### 2.7. The 6°05′W data

The five profiles performed at 6°05′W during each campaign that were deep enough to possibly sample the MWs are displayed in both Figs. 18 and 15b, which allows comparisons with those at 5°50′W in Figs. 16A and 15a. During GIB1, profile #1 is colored in violet and red since it is slightly but significantly different from the red group #2–3 that clearly indicates LIW while #4 indicates WIW. As at 5°50′W and further upstream, no profile can be associated with WMDW. During GIB2, the associations #1-WMDW (note the undulated shape), #2–3-TDW and #4-WIW are clear, especially from Fig. 15b. No profile indicates LIW, which is consistent with the low amount of mixed LIW at 5°50′W and further upstream; as suggested by data downstream, the small LIW suboutflow was probably missed there. Similarly, and as demonstrated by the differences between #2 and #3 that both sampled the TDW suboutflow with inaccuracies similar to those already noticed at 5°50′W for #1–2/GIB2 (#3 is markedly deeper than #2), the WMDW suboutflow was not accurately sampled by profile #1 and must clearly be denser (in fact, the densest). Also note that #1/GIB1 did not correctly sample the TDW suboutflow and that there is a relatively

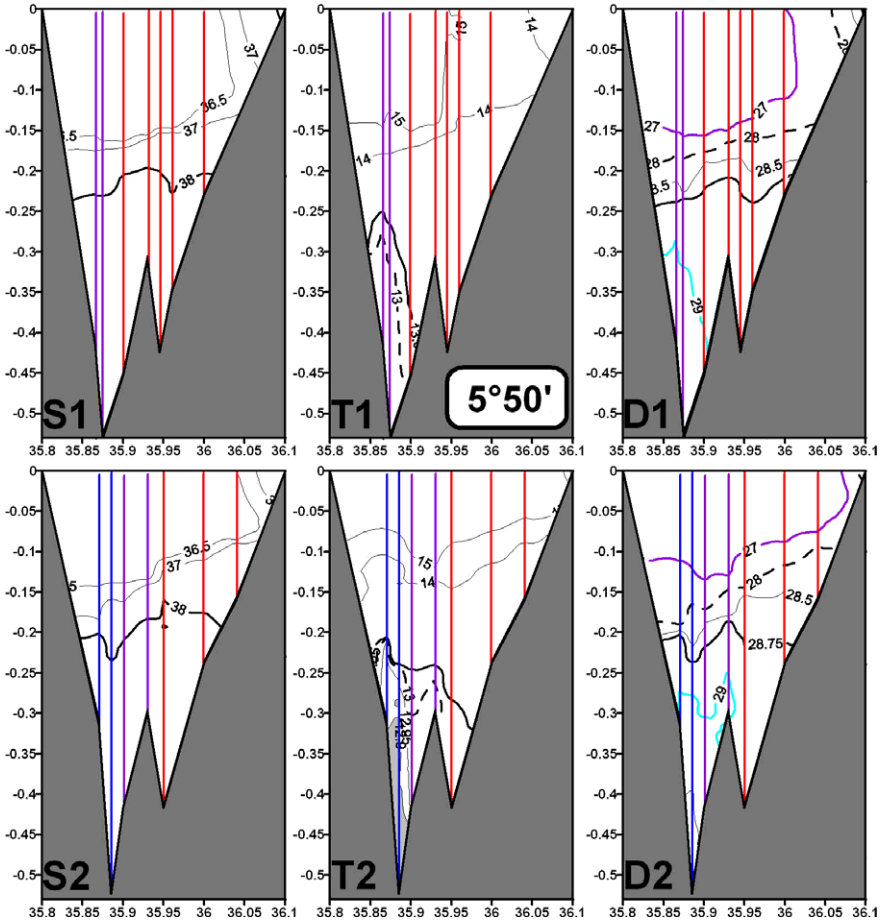


**Fig. 17.** Same as in Fig. 5 for 5°50′W. $\sigma = 27.0$ kg m$^{-3}$ is violet and $\sigma = 29.0$ kg m$^{-3}$ is cyan. (For interpretation of the references to colour in this figure legend, the reader is referred to the web version of this article.)

large spacing between #1 and #2 during GIB2, which might indicate that the sampling interval there was not small enough. During LYNCH12, #2–3 indicate mixed LIW and #4 mixed WIW while during LYNCH34, consistent with the data at 5°50′W, #2 (performed in triplicate) once indicates WMDW, all other profiles indicating either more mixed WMDW or LIW.

The large spatial variability during all campaigns and the large temporal variability indicated by the LYNCH data illustrate the difficulty of correctly sampling there. Additionally, separating AW–MWs mixing lines for two different MWs depends on the nature of AW. For instance, NACW–TDW and NACW–WMDW lines are separated while the SAW–TDW and SAW–WMDW ones are superposed (the reverse occurs for WIW and LIW). It is thus obvious that a suboutflow can be either missed or mistaken with another one, and that the extrema are clearly depth dependent (those indicated by a unique-profile being unreliable). However, let us assume that the extrema associated with all the MWs during both GIB campaigns (except WMDW not correctly sampled during GIB2) are representative of the actual ones. Even though the outflow composition during GIB1 (WIW, LIW, TDW, no WMDW) and GIB2 (WIW, little LIW, TDW, WMDW) was markedly different, each of the MWs was characterized by extrema that were shifted from 5°50′W to 6°05′W along the mixing lines with AW, which supports the coloring. The $\sigma_{max}$ shift is ~0.1 kg m$^{-3}$ for TDW and LIW, ~0.2 kg m$^{-3}$ for WIW. Note that $\Delta\sigma_{max}$ between the two densest suboutflows (TDW and LIW during GIB1, WMDW and TDW during GIB2) differ by 0.1–0.2 kg m$^{-3}$ while the range for all MWs is $\Delta\sigma$ = 0.2–0.3 kg m$^{-3}$ (associated with $\Delta\theta$ = 0.2–0.3 °C, $\Delta S$ = 0.2–0.3). Ranges at a given location for the densest suboutflows (between TDW–GIB1 and WMDW–GIB2 or between LIW–GIB1 and TDW–GIB2) are about half these values. Even though characterizing a priori a given suboutflow by specific hydrographic values corresponding to a given MW is impossible, the southernmost (respectively northernmost) suboutflow expected to be actually the denser (lighter) might always be relatively cool (warm), compared to the neighboring ones, which would correspond to the observations about the veins downstream. Assuming a homogeneous outflow was certainly hypothesized for convenience but has never been supported by any data set, and no data sets is more detailed or can be considered as more reliable than the GE one, even if still not accurate enough.

GIB1 and GIB2 are not very informative about the densest/southernmost suboutflow (Fig. 18) that is indicated by only one (#1) non-very representative profile. Overall largest densities were certainly missed: during GIB1, they were due to TDW and thus probably south of #1 since #1 is still relatively similar to #2–3 that indicate LIW; during GIB2, they were due to WMDW and thus probably between #1 and #2 since corresponding depth must be greater than at #1. During both LYNCH12 and LYNCH34, the densest/southernmost suboutflow is indicated by profiles #2 mainly since #1 is either out of range or indicative or more mixed water while #3–4 indicate either the same MW more mixed or another MW. We thus expect this suboutflow and other ones as well to have moved toward the central part of the transect, which is somehow supported by the sections (Fig. 19). Apart from the NACW intrusion at 200–250 m during GIB2 (leading to the undulations on #1, Fig. 18), and even though overall maximum densities associated with the southernmost/densest suboutflow were certainly missed, the deep isopycnals tend to flatten (GIB1) or even to tilt up northward (GIB2).

### 2.8. The 6°15′W data

Among the four/eight GIB1/GIB2 profiles (Fig. 20), only two/three of the profiles sampled the outflow now found in the lower part of the northern/Iberian continental slope, which confirms the displacement of the densest MWs from the southern slope (~5°50′W) to the central part of the strait (~6°05′W) and finally to the northern slope (~6°15′W). Such a limited number of profiles does not allow statistically significant results but they provide extremely valuable information. Since the $S_{max}$ found at 400–600 m near 6°30′W is $S \sim 37$ (Borenäs et al., 2002), we focus on larger values. $\theta$–$S$ diagrams (Fig. 21) are no longer straight mixing lines and display marked undulations. These major changes prevent coloring the profiles as done upstream but, more interestingly, several comments support coloration by undulation.

A mid-depth undulation such as the bump identified by a continuous line on the #6/GIB2 $\theta$–$S$ diagram (Fig. 21b) indicates $\theta$ and $S$ relative maxima. This bump's general shape is similar to that of any diagram displaying LIW in the sea or the whole outflow in the ocean so that it characterizes an intermediate vein of relatively warm salty water. Other mid-depth bumps that do not have relative maxima depict a more mixed vein, or at least intrusions, of MWs into AW. Successive bumps on a given diagram thus indicate overlying veins or intrusions that are supposed contiguous. The lowest parts of the #3/GIB1 and #5–6–7/GIB2 diagrams are markedly bended and represent the upper part of such bumps. Because profiles covered nearly all the water column, these half-bumps indicate actual veins still flowing over the bottom.

We assume that (i) the suboutflows upstream (at 5°50′W (Fig. 16A) and 6°05′W (Fig. 18)), which are consistent with the MWs amounts east of the sill, cascade individually and lead to specific veins at 6°15′W, (ii) all significant suboutflows upstream and veins at 6°15′W were sampled so that each MW presence/absence is consistent in the whole study area, (iii) the suboutflows and veins $\sigma_{max}$ are not accurately defined, in particular with only one profile, and the densest suboutflow (respectively vein) is the southernmost (respectively deepest) one, (iv) veins flow along the northern slope at 6°15′W, as expected for any density current (Fig. 20), (v) when sampling a warm salty vein with profiles approaching its core, all characteristics ($\theta$, $S$ and $\sigma$ regularly increase, so that links exist between bumps on neighboring profiles (Fig. 21). The quite satisfying coloration we came with is: WIW (pink) during GIB1 and GIB2, LIW (red) mainly during GIB1 and both mixed and in small amount during GIB2, TDW (violet) during both GIB2 and GIB1, WMDW (blue) during GIB2 only. When comparing GIB1 and GIB2, a major remark concerns the TDW $\sigma_{max}$. During GIB1, TDW is the densest vein and its $\sigma_{max}$ reduces only slightly (by ~0.2 kg m$^{-3}$) from 5°50′W (where it is well defined) to 6°15′W, roughly as much as the WMDW $\sigma_{max}$ during GIB2 (reducing ~0.25 kg m$^{-3}$). During GIB2, TDW is no more the densest vein and its $\sigma_{max}$ reducing is larger (by ~0.5 kg m$^{-3}$). A similar remark concerns the LIW $\sigma_{max}$ that reduces only by ~0.5 kg m$^{-3}$ when unmixed and in large amount (GIB1) and by ~0.7 kg m$^{-3}$ when mixed and in small amount (GIB2). The WIW $\sigma_{max}$ reduced by larger amounts. Overall and as expected, the mixing of a vein with AW is inversely proportional to its depth an amount: the greater the depth and amount, the lower its $\sigma_{max}$ reducing.

The colored bars in Fig. 20 confirm these hypotheses since the pink, red, violet and blue layers have realistic thicknesses and mean depths on the various profiles during both GIB1 and GIB2. The non-occurrence of any red-LIW bump on #4/GIB1 that would be expected from the #3 bump leads to a relatively thick pink layer there, which might be due to small-scale heterogeneity. The #7/GIB2 red-LIW half-bump is not retrieved on #5–6, which is consistent with the LIW/GIB2 small amount. Quite surprisingly, both WIW and TDW that were almost never mentioned in current thoughts (Section 1.1) represented large percentages of the outflow during both GIB1 and GIB2. Quite surprisingly too, LIW and WMDW that are currently thought as being the sole components of the outflow can represent a low percentage (LIW during GIB2) or be absent (WMDW during GIB1).

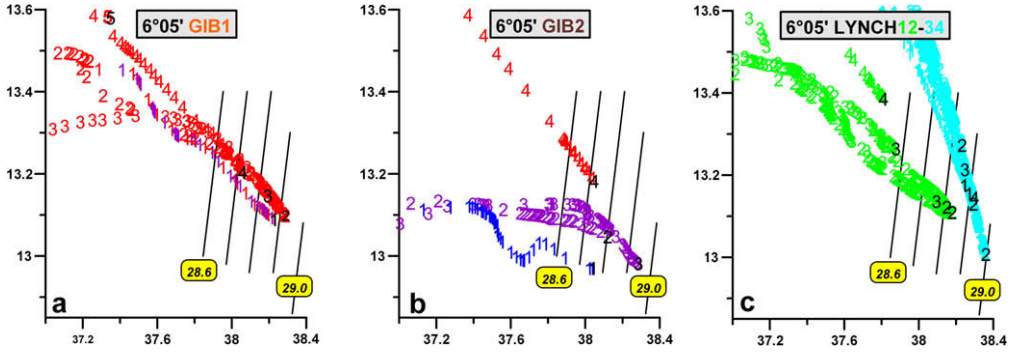


**Fig. 18.** Same as in Fig. 16A for 6°05′W.

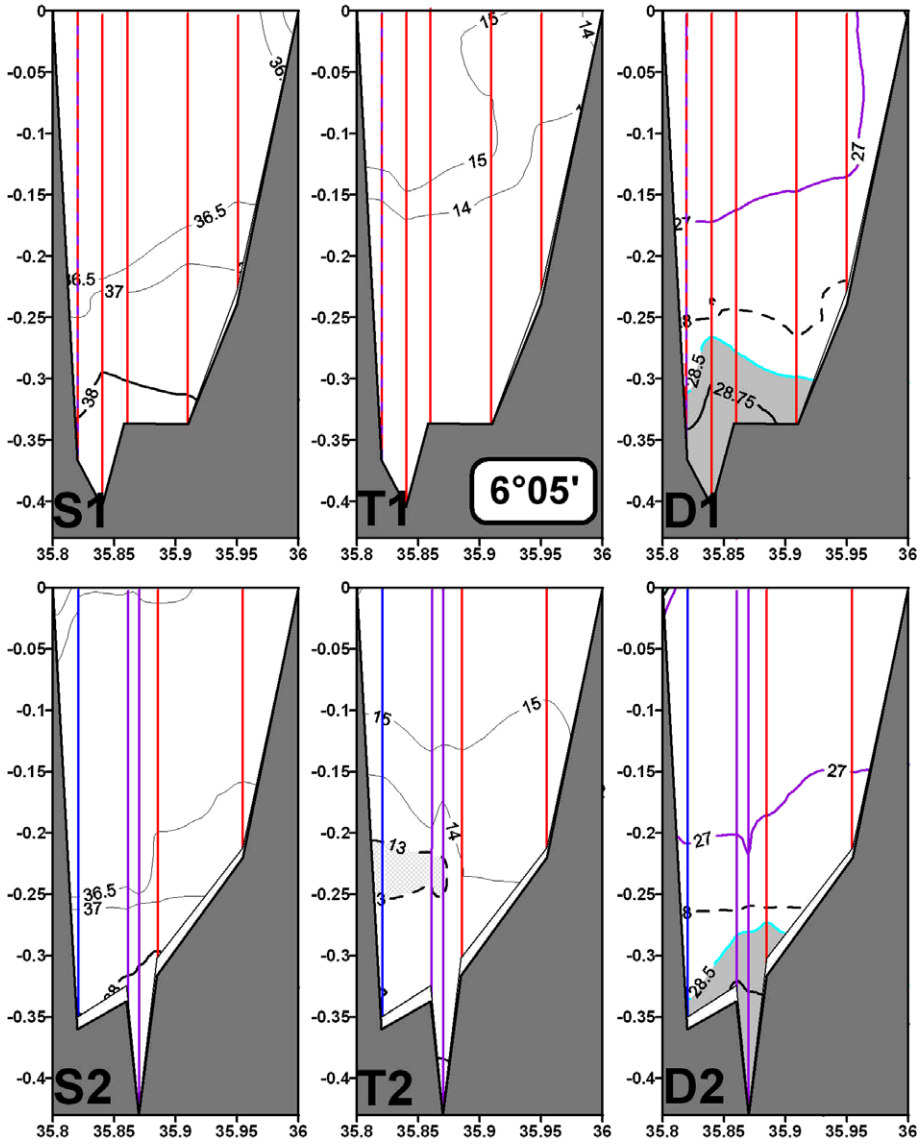


**Fig. 19.** As in Fig. 5 for 6°05′W. Densities >$\sigma$ = 28.5 kg m$^{-3}$ (cyan) are in grey, $\sigma$ = 28.75 kg m$^{-3}$ is thick, $\sigma$ = 27.0 kg m$^{-3}$ is violet. (For interpretation of the references to colour in this figure legend, the reader is referred to the web version of this article.)

Fig. 21 shows that the two densest veins $\sigma_{max}$ (GIB1: TDW and LIW, GIB2: WMDW and TDW) differ by a similar $\Delta\sigma_{max} \sim 0.3$ kg m$^{-3}$ even though the GIB1-$\sigma_{max}$ are slightly larger than the GIB2-$\sigma_{max}$ ones. Since this difference at 6°15′W corresponds to those reported 100–200 km downstream when the veins no longer cascade and are characterized by $\sigma_{max}$ lower by $\sim$1.0 kg m$^{-3}$, it might be that the densest veins similarly mix downstream. Even though the densest veins correspond to differ-

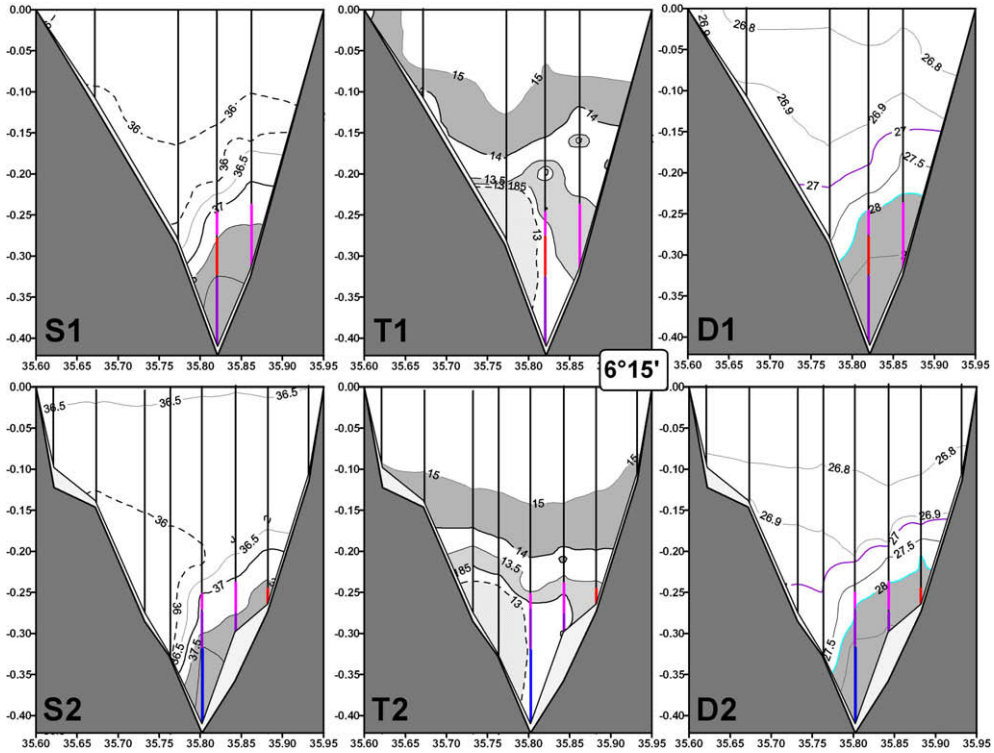


**Fig. 20.** As in Fig. 5 for 6°15′W and specific isolines. $S$ = 36.0 (dashed) emphasizes the AW $S_{min}$, $S$ = 37.0 (thick) represents the AW–MWs interface, $S$ > 37.5 (grey) represents unmixed MWs, the largest isoline value is $S$ = 38.0. In T1 and T2, $\theta$ < 13.0 °C (dashed) are in lattice grey, $\theta$ = 13.185 °C (thick) locates the vein on the bottom at #6/GIB2. In D1 and D2, $\sigma$ = 27.0 kg m$^{-3}$ (violet) represents the AW–MWs interface, $\sigma$ > 28.0 kg m$^{-3}$ (cyan) are in grey, the largest isoline value is $\sigma$ = 28.5 kg m$^{-3}$. (For interpretation of the references to colour in this figure legend, the reader is referred to the web version of this article.)

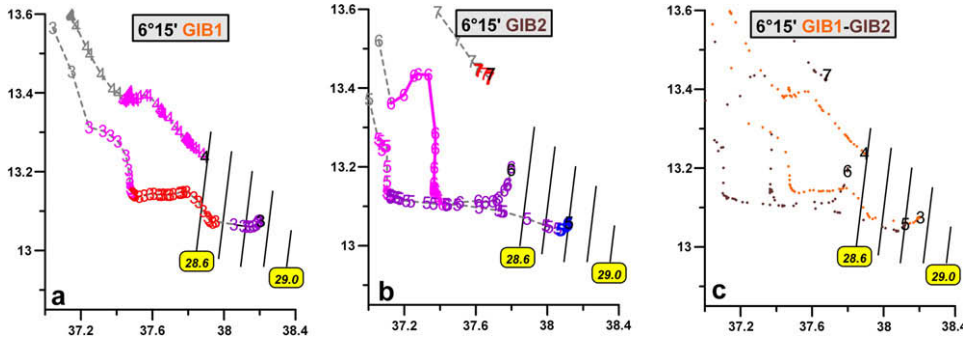


**Fig. 21.** $\theta$–$S$ diagrams at 6°15′W for GIB1 (a), GIB2 (b) and both (c) showing WIW (pink), LIW (red), TDW (violet) and WMDW (blue). Isopycnals are 0.1 kg m$^{-3}$ apart. (For interpretation of the references to colour in this figure legend, the reader is referred to the web version of this article.)

ent MWs, the deep vein is ~90-m thick and the intermediate one is 50-m thick during both GIB1 and GIB2. Furthermore the two veins have roughly similar $\theta$ and $S$ even though associated with different MWs, this clearly explains the permanency of the veins characteristics currently assumed. The third upper vein described in the literature is the WIW vein (possibly confused with the LIW one as during GIB2), it is consistently the warmest, and $\Delta\sigma_{max}$ are within the reported ranges.

During GIB1, the $S$ section (Fig. 20) also shows the AW $S_{min}$ (<36.0) spreading over the whole transect. The low $\theta$ values at the base of the southern/Moroccan slope indicate NACW and some relative maxima over the northern slope indicate heterogeneities due to the AW–MWs interactions, while all densest isopycnals are tilting up northward. During GIB2, the AW $S_{min}$ is less spread and the MWs $S_{max}$ values are slightly lower. The $\theta$ section still indicates NACW, which might be a frequent (if not permanent) feature, together with numerous heterogeneities.

## 3. The 80-m and 270-m time series analysis

The HCP data are presented in Section 1.2. Major results concerning the composition and spatio-temporal variability of the MWs outflow are displayed with a series of $\theta$–$S$ diagrams allowing comparisons between the data at both locations over time. The number of diagrams/periods (six for the 2003–2007 time series) is a compromise allowing a relatively large number of diverse situations to be differentiated (Fig. 22). The selection made from a visual analysis only is validated by the large variability. As expected from the GE transects analysis, only LIW, TDW and WMDW (not WIW) were found at the sill and/or on the Moroccan shelf, so that only the upper part (38.44–38.52) of the MWs $S$-range is of interest. Similarly, the MWs $\theta$-range is reduced to 12.92–13.25 °C since (i) the lowest $\theta$ are generally located along the Moroccan slope, i.e. neither at the sill nor on the shelf, (ii) marked changes have occurred in the sea, and/or (iii) the oceanic trends are generally posi-

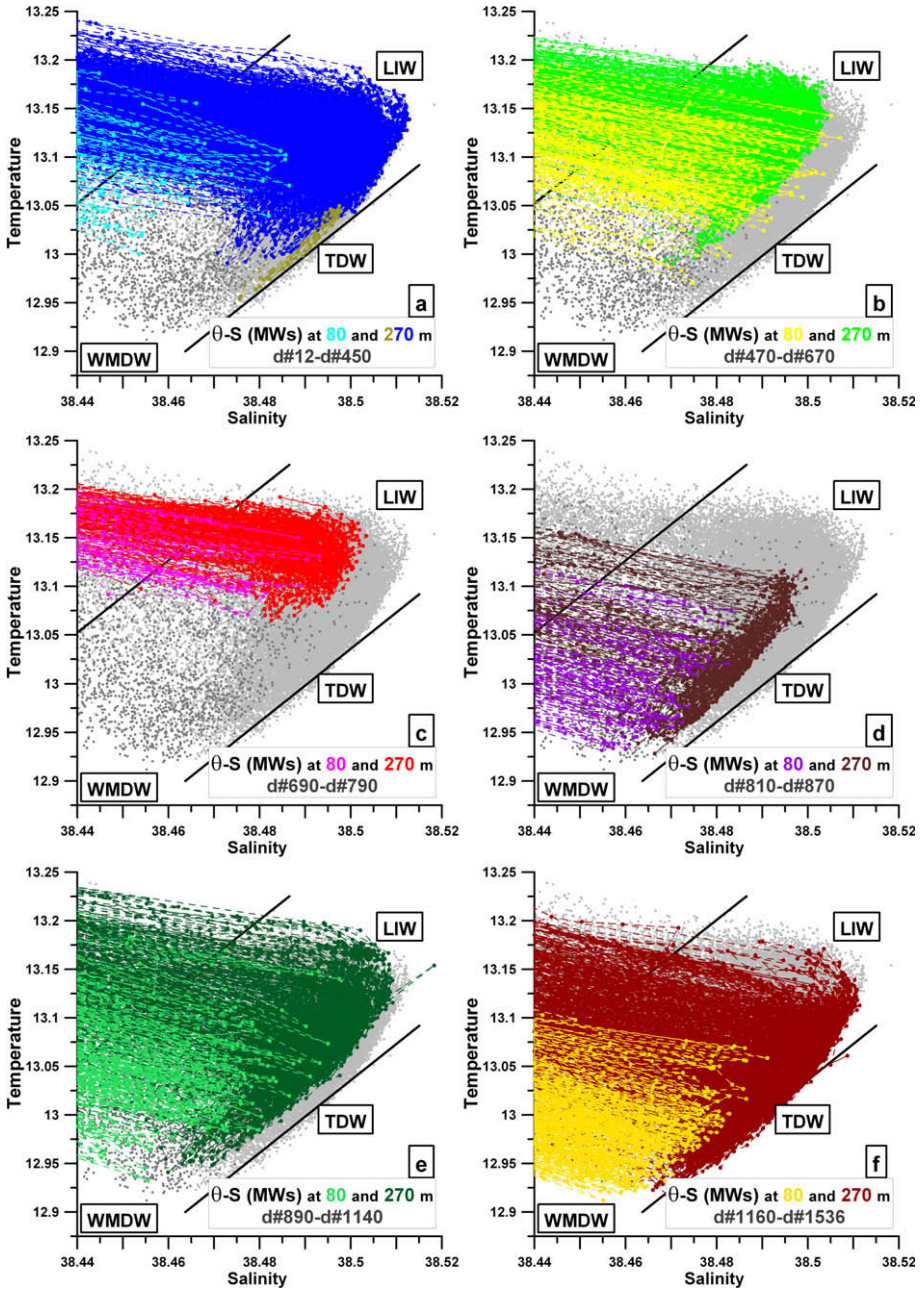


**Fig. 22.** $\theta$–$S$ diagrams from the 2003–2007 (Julian days #12–1536) time series at 270 and 80 m and the six periods (a–f) specified in the text. The whole time series are plotted with light grey dots (270 m) and dark grey ones (80 m), together with $\sigma$ = 29.05 and 29.10 kg m$^{-3}$. The colors significance and the date intervals for each of the periods are specified in both the text and the figure. Dashed lines connect consecutive data and provide information about mixing. (For interpretation of the references to colour in this figure legend, the reader is referred to the web version of this article.)

tive. Because TDW (i) cannot be clearly differentiated from LIW above and WMDW below, (ii) is not characterized by any extremum and (iii) is often encountered at 270 m, terms such has lower, central and upper parts of a unique TDW-range (on such diagrams) are used to deal, as precisely as possible, with TDW being more or less dense (over time). Both NACW and SAW were measured at 80 m (not shown). Days are Julian days from January 1st, 2003, and successive periods are separated by 20 days to avoid confusing situations.

Days #12–450 (Fig. 22a). At 270 m, relatively high $\sigma$ (29.095–29.100 kg m$^{-3}$) and $S$, associated with either TDW or LIW, occurred during this period (blue points). This is particularly obvious when TDW unmixed with either AW or any other MW was continuously observed during the three first days (gold), so that more extreme situations probably occurred before. Even though this was during neaps (Section 4.1), this suggests a relatively intense TDW outflow. As shown by several dashed lines nearly parallel to isopycnals >29.08 kg m$^{-3}$ for central-TDW (also for upper-TDW and LIW, unclear in the figure), MWs unmixed with AW were often observed during several consecutive records. However, mixing with AW (lines nearly perpendicular to the isopycnals) due to the internal tide was generally significant at the sill (even when the most homogeneous LIW outflowed), hence for the whole MWs outflow. No points indicative of either lower-TDW or WMDW were observed during this 440-day period. At 80 m, points (cyan) were very rare (they were never so rare thereafter) and they all indicated intense mixing with AW. Compared to points at 270 m, points at 80 m were generally more shifted toward the lower left part of

the diagram, which is a 80-m vs. 270-m difference often encountered hereafter. Links exist between the MWs found at both locations and between the facts that large densities occurred at the sill when few MWs occurred on the shelf.

Days #470–670 (Fig. 22b). At 270 m (green), either LIW or upper- and central-TDW were still encountered, sometimes not mixed with AW during several consecutive records but now with markedly lower *S*. Values at 80 m (yellow) were sometimes denser than at 270 m, still associated with either LIW or TDW but in less mixed conditions. Compared to those during the twice-longer period #1, 80-m points were more numerous. But similarly, 80-m points were more shifted towards cooler and fresher waters than 270-m ones. Points signed mainly TDW (upper, central and lower) at 80 m, and mainly LIW and upper + central (lower is rare) TDW at 270 m. Links exist between relatively light MWs at the sill and much denser MWs on the shelf.

Days #690–790 (Fig. 22c). Only LIW, more or less mixed with AW, was found at 270 m (red) with $\theta$ and *S* values significantly lower than during the two previous periods while only LIW (and/or upper-TDW) more mixed with AW was found at 80 m (pink). Since the densest waters (lower-TDW and WMDW), generally located along the Moroccan slope, were not sampled at any place, they were either absent or present in a limited amount. Such a situation, with no (observed) or little (possibly outflowing) dense MWs from either the eastern basin (TDW) or the western one (WMDW), has never been encountered since.

Days #810–870 (Fig. 22d). Dramatic changes have now occurred at both 270 m (brown) and 80 m (violet). At 270 m, upper- to lower-TDW and rare WMDW were found in relatively unmixed conditions, as indicated by the low number of AW–TDW and AW–WMDW mixing lines as compared to the number of lines roughly parallel to the isopycnals (clear at least for upper-TDW). At 80 m, mainly WMDW and lower- to central-TDW were found in more mixed (less salty at least) conditions. From the beginning of the experiment, it is the first time that no LIW was recorded, that lower-TDW was relatively frequent, and that WMDW was present at both locations, which indicates an outflow mainly of western origin. The mainly eastern origin has lasted for ~800 days at least, probably more since the situation at the beginning of the experiment was relatively extreme. Changes about WMDW mainly, which were observed from this mid March to mid May 2005 period and later on, could be due to the large amount of WMDW formed during that winter in the Provençal subbasin (Fuda et al., 2007).

Days #890–1140 (Fig. 22e). The situation markedly changed again since now all three MWs (LIW, TDW and WMDW) were measured at both 270 m (dark green) and 80 m (light green). They were mixed either together (clear for lower-TDW and WMDW) or with AW at 270 m while there were mixed only with AW at 80 m. Characteristics of both LIW and upper-TDW at 270 m were less extreme (warm and salty) than during period #1 (and #6), but together with the characteristics of the lower-TDW, they were more pronounced (saltier at least) than during periods #2–3–4. Most of the MWs at 80 m can be considered as a mixture of those at 270 m. But as during period #4, the coolest values sign WMDW never found at 270 m.

Days #1160–1536 (Fig. 22f). Period #6 at 270 m (brown) is characterized by upper-TDW similar to that encountered during period #1, and by central- to lower-TDW more abundant and even denser (<29.104 kg $m^{-3}$) than during period #1, together with less LIW and more WMDW. At 80 m (orange), mainly WMDW, central- and lower-TDW occurred. Note that, overall, the less mixed (i.e. densest) central- to lower-TDW (at 270 m) and WMDW (at 80 m) were observed simultaneously during this period.

Days #1536–1760 (not shown). Even though the CTDs used from March 2007 to October 2008 are not post-calibrated yet, the continuity of the time series from before to after day #1556 accounts for the accuracy of the data shown in Fig. 22f in particular. During this 220-day period, data at 270 m suggest the occurrence of upper- to lower-TDW as in Fig. 22d and e while data at 80 m in the displayed ranges are even more rare than in Fig. 22a. Assuming corrections similar to those previously made would not dramatically change these features, which would illustrate another situation never encountered up to now.

## 4. Discussion

Complementary analyses provide a more detailed description of the MWs outflow. A current meter at 270 m allows specifying some aspects of its short-term variability (Section 4.1). Statistics on the 4-year long time series at 270 m provide significant information on its seasonal variability (Section 4.2). A synthesis of the results obtained with the time series at both 80 m and 270 m allows specifying its long-term variability (Section 4.3). The low mixing of the light MWs up to the sill and the continuous evolution of the outflow structure meanwhile allow simple computations that explain some of the current thoughts and quantify the GIB1 vs. GIB2 differences (Section 4.4). Finally, a new concept of the MWs outflow is proposed with the major aim to motivate as many as possible further studies (Section 4.5).

### 4.1. Short-term variability

A RCM9 Aanderra current meter set at 270 m worked for ~6.5 months in early 2003. One-hour velocities (*V*), all measured in the 225-45 T direction, ranged from +190 cm $s^{-1}$ (towards 225 T) to −135 cm $s^{-1}$ due to the large semi-diurnal variability. The daily (25-h) moving average of *V* (Fig. 23) displays a well-known (Candela et al., 1990) fortnightly signal locked on the tide at Tarifa with maximum deep-sill current during neaps, which is consistent with the largest outflow at springs (Bryden et al., 1994; Vargas et al., 2006). The CTD data allow plotting $\sigma$ as grey and cyan dots, the latter resulting from a selection based on a criterion explained in Section 4.2. The *S* (38.32–38.51) and $\theta$ (13.0–13.25 °C) curves are almost identical (*S*) or similar ($\theta$, descending axis) to the $\sigma$ one.

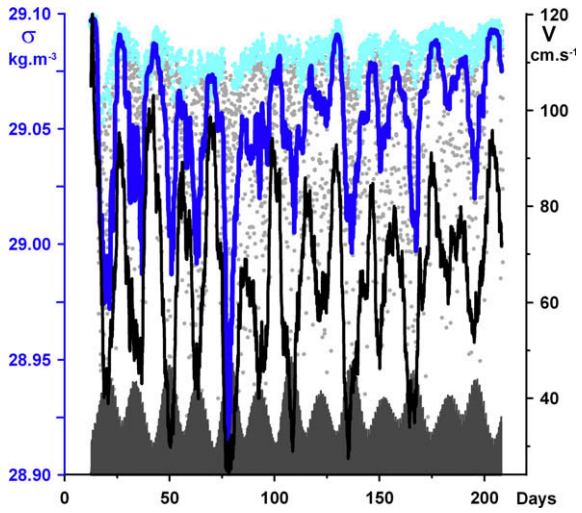


**Fig. 23.** Density ($\sigma$) data measured (grey dots) and selected with the sd criterion (cyan dots) for the MWs at 270 m from January 12 to July 27, 2003, together with the daily moving averages of the measured density (blue curve) and speed (V) toward 225 °T (black curve); tidal amplitude at Tarifa (maxima ~80 cm) is from Julio Candela (personal communication). (For interpretation of the references to colour in this figure legend, the reader is referred to the web version of this article.)

The $\sigma$ and $V$ curves are in phase, the densest less-mixed MWs rapidly outflowing during neaps. During days #12–14, the largest $\sigma$ measured at the beginning of the experiment (Fig. 22a, gold points) lead to daily averages >29.096 kg m$^{-3}$, and $V$ was the largest ever measured too (~120 cm s$^{-1}$ on day #13, 4-day average ~100 cm s$^{-1}$). Such a rapid outflow of dense MWs, even if maybe of limited vertical extent, probably represented a significant part of the whole outflow. Near day #80, the lowest $\sigma$ (~28.90 kg m$^{-3}$) were associated with the lowest $V$ (~25 cm s$^{-1}$), such a slow outflow of relatively light MWs probably not significantly modifying the whole outflow. Note that no $\sigma$ values were selected at this time by the criterion. The huge fortnightly variability of the hydrographic parameters at the sill is obviously larger at shallower depths across the whole strait, which leads to a significant signal all along the outflow downstream that has never been looked for.

During this 6.5-month period, and even though variations induced on both $\sigma$ and $V$ by the tide and other unknown or unresolved forcings are relatively large, $\sigma$ data selected for the MWs were still in a relatively high range (29.05–29.10 kg m$^{-3}$) while the overall mean $V$ = 66 cm/s, which is a relatively large value as compared to other published ones (e.g. Bryden et al., 1994). These features are used to explain the differences we make thereafter between an overflow and an outflow.

### 4.2. Seasonal variability

We do not expect any seasonal variability of the MWs outflow up to the sill (see Section 1.2), contrary to what occurs for the AW inflow (Millot, 2007). The 4-year long and 1-h time series (36,600 data) at 270 m, where points representative of the MWs are more numerous and less dependent on tidal mixing than at 80 m, allows some objective and probably significant analysis. We address the seasonal variability first with a standard fitting of the 270-m time series, then with a method we are elaborating and already applied to the 80-m one (Millot, 2007).

The curves in Fig. 24 represent the polynomial fits to sets of $\theta$, $S$ and $\sigma$ data selected in different ways for each of the four years starting in January 2003. The polynomial degree (three) and 1-year periods are a priori able to detect any almost regular/sinusoidal signal. The black curves are for all points in the MWs ranges used for Fig. 24 (38.44–38.52, 12.90–13.25 °C, 29.06–29.10 kg m$^{-3}$), which selects numerous points indicative of AW–MWs mixing. The red curves are from points selected according to a tidal criterion, i.e. retaining only the $\theta_{min}$, $S_{max}$ and $\sigma_{max}$ for each consecutive semi-diurnal (12-h) period, which gives 3050 regularly distributed points that can still be influenced by AW–MWs mixing, particularly during springs. The blue curves are from the sets of 3050 points selected according to a standard deviation (sd) criterion. A sd being computed over some (three) consecutive data and associated with the central one, only the data for which the sd is lower than some arbitrarily-fixed maximum value are retained, which allows selecting data representative of the most homogeneous MWs at one's convenience.

For all three parameters, relatively similar "seasonal" variations are observed during years #1–2 on one side, and during years #3–4 on the other side. The former are very different, if not opposed, to the latter. The corrected time series ending in March 2007, we did the same analysis over four years with a 2-month shift, as well as over three years with a 6-month shift. We also conducted similar analyses with the 80-m time series. All three time-intervals lead to the same conclusion at both 80 and 270 m, i.e. that S, $\theta$ and $\sigma$ for the MWs do not show any kind of seasonal variability.

Interesting information is provided by the distribution with time of the data selected with the sd criterion. Relatively unmixed AW and MWs being defined by specific ranges (AW: $S < 37$, $\theta > 13.5$ °C; MWs: $S > 38.4$, $\theta < 13.25$ °C), frequencies of occurrence for both waters are about 67% and 8% at 80 m, 0% and 92% at 270 m. One can then consider, for both AW and the MWs, the distribution with time (1-month averages) of the most homogeneous data (i.e. having the lowest sd; we arbitrarily chose the 30% most homogeneous) in S, $\theta$ and $\sigma$, as well as of the so-called triplets that correspond to the sets of data selected at the same time for all three parameters. Considering other realistic ranges for either AW or the MWs, and/or computing the sd over two or four consecutive values, and/or selecting slightly more (i.e. 40%) or less (i.e. 20%) homogeneous data does not basically change the results displayed in Fig. 25.

For the AW at 80 m (Fig. 25a), the distribution with time of the 7320 data (30% of 67% of the 36,600 available data) selected for all three parameters, and of the 4437 triplets that result from this selection, displays a marked seasonal variability. Most homogeneous data and numerous triplets occur during the second half of February (dashed lines). This is linked to the meteorological conditions in the study area and the wintertime mixing of any surface layer that leads to the $S$(AW) seasonal variability (Millot, 2007). As confirmed by a sharper selection (i.e. less than 30%) the interannual variability is significant too.

For the MWs at 80 m (Fig. 25b), the distribution of the 915 data (30% of 8%) and of the 695 triplets displays marked seasonal and interannual variabilities. The seasonal variability appears as a peak occurring well after the AW peak, i.e. when AW starts re-stratifying and no longer mixes with the MWs as during the winter, allowing unmixed MWs to be often sampled. Then, seasonal stratification reaches the MWs layer and lowers the number of homogeneous data. The interannual variability mainly shows the non-occurrence in 2003 and the rare occurrence in early 2004 of the MWs (Fig. 22a). The similarity between the curves for the three parameters yields to a relatively large number of triplets not related to

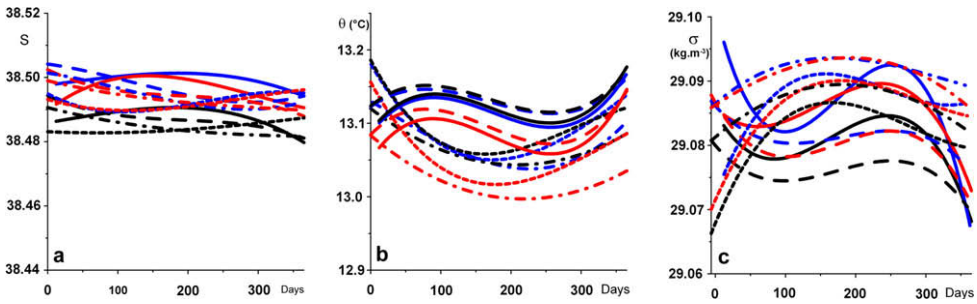


**Fig. 24.** Polynomial (degree 3) fits from the $S$ (a), $\theta$ (b), and $\sigma$ (c) data at 270 m during year #1 (full line), #2 (large dashed line), #3 (small dashed line) and #4 (dashed dotted line). Black lines correspond to the whole set of data measured in the MWs displayed ranges. Red lines correspond to regularly distributed data selected with a tidal criterion ($S_{max}$, $\theta_{min}$ and $\sigma_{max}$ over 12-h successive intervals) while blue lines correspond to the same amount of data selected with the sd criterion (hence irregularly distributed). (For interpretation of the references to colour in this figure legend, the reader is referred to the web version of this article.)

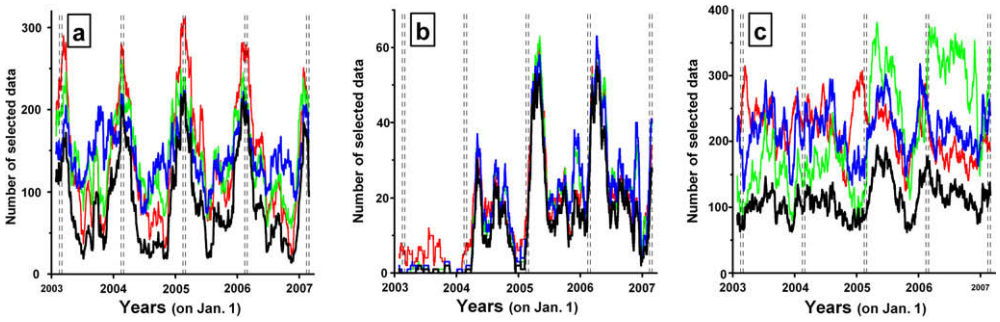


**Fig. 25.** Monthly moving averages of the number of $S$ (blue), $\theta$ (red) and $\sigma$ (green) data selected with the sd criterion (30%) for AW at 80 m (a), the MWs at 80 m (b) and the MWs at 270 m (c); corresponding triplets are in black. The more homogeneous AW is encountered in the second half of February (dashed lines). See text and Millot (2007) for details. (For interpretation of the references to colour in this figure legend, the reader is referred to the web version of this article.)

some specific character of the MWs there. Rather, the scarcity of unmixed MWs leads to select data influenced by mixing with AW, hence distributed, in a $\theta$–$S$ diagram, along lines roughly perpendicular to the isopycnals. Standard deviations for all three parameters are thus proportional, leading data to be selected at the same time. The large interannual variability prevents from evidencing the seasonal variability with a polynomial fit.

For the MWs at 270 m (Fig. 25c), the distribution of the 10980 data (30% of 92%) and of the 5651 triplets displays a marked interannual variability (see Section 4.3) with no seasonal variability. This is obviously representative of most of the outflow approaching the sill. However, tidal mixing with AW at the sill is intense (e.g. Figs. 22 and 23), characteristics of the outflow downstream from the sill markedly depend on AW in the sill surroundings (e.g. Fig. 18c) and AW displays a marked seasonal variability (Fig. 25a). Therefore, the MWs outflow in the ocean should display a seasonal variability imposed, via mixing with AW in the sill surroundings, by the meteorological forcing.

### 4.3. Long-term variability

Fig. 25c also indicates that the three parameters at 270 m have non-related variations and relatively similar and constant mean levels in 2003–2004 while they have larger and sometimes more similar variations with different levels in 2005–2006. The MWs in 2003–2004 were more homogeneous in $S$ and $\theta$ than in $\sigma$ while, in 2005–2006, they were more homogeneous in $\sigma$ than in $S$ and $\theta$, which is related to the general shape of the $\theta$–$S$ diagrams (Fig. 22) that were more aligned with the isopycnals during the second half of the experiment. The large number of homogeneous $\theta$ at the end of 2004 corresponds to period #3 with only LIW (Fig. 22c). The simultaneity of some 270-m peaks in 2005 might be fortuitous since they are not simultaneous in 2006.

Considering the LIW and upper-TDW vs. WIW amounts, as well as the lower-TDW vs. WMDW ones, the GE data show that the outflow can be more of eastern (GIB1) or western (GIB2) origin. Consistently, blue profiles (Table 1) were never observed during GIB1 while observed on all transects during GIB2. Both campaigns also show that, in the sill surroundings, the MWs are more juxtaposed than superposed, the denser further south, and that all MWs mix more with AW than together. Finally, the light–dense MWs interface ($\sigma$ = 29.08 kg m$^{-3}$, Fig. 3) markedly tilts east of the sill, up to being nearly parallel to the southern continental slope, during both GIB1 and GIB2. Such information about the outflow long-term variations and cross–strait distribution currently inferred from CTD profiles is fully consistent with that inferred from the less standard CTD time series.

Before comparing the six periods defined for the 2003–2007 HCP experiment (Fig. 22), some points must be specified. Time series at 80 m on the Moroccan shelf and at 270 m near Camarinal Sill South do not generally indicate the densest MWs that are expected (from e.g. the GE data) to be at 200–300 m along the Moroccan slope. Such time series do not provide information about WIW that always outflows more to the north at shallower depths. The LIW $S$ and $\theta$ overall maxima in 2003–2007 at 270 m and 5°45′W (>38.51, >13.15 °C) were encountered ~20 years ago in the western Alboran but never expected to be measured at the sill (Millot et al., 2006). A 1984 one-week time series at the sill (294 m; Pettigrew, 1989), i.e. close to our 270-m site, regularly indicated $\theta$ < 12.9 °C, hence relatively unmixed WMDW, while we measured only ~100 values out of ~36600 in a higher range of 12.92–12.95 °C and only during the second half of the experiment.

Main characteristics during period #1 (~440 days, Fig. 22a) are the occurrence of relatively large densities at 270 m associated with TDW (not WMDW) and the scarcity of points at 80 m mainly showing mixed TDW (not WMDW). This makes unlikely the outflow of a significant amount of WMDW along the slope in between. When considering the large speeds at 270 m, we expect (without any proof) the isopycnals to have been either horizontal or tilting up northward. Such a situation illustrates what we call an overflow.

An almost opposite situation occurred during period #2 (~200 days, Fig. 22b) with relatively low densities at 270 m, associated with either LIW or TDW, and relatively numerous points at 80 m sometimes indicating either LIW or TDW denser than at 270 m. There is little chance of finding a WMDW outflow in between. However, denser TDW was certainly outflowing along the slope since AW–MWs mixing is lower there than on the shelf. Such a situation indicating a relatively large tilting up of the MWs isopycnals southward is the most extreme we encountered.

Another extreme situation occurred during period #3 (~100 days, Fig. 22c) with only relatively mixed LIW at both 270 and 80 m, hence probably leaving no place in between for some TDW or WMDW outflow. One can think either that a core of less mixed LIW is outflowing more to the north, making LIW the dominant component of the outflow, or that a relatively large amount of WIW is outflowing too, hence pushing the LIW core away from the northern slope, as during GIB2.

Dramatic changes then occurred since no LIW at all was observed at either 270 or 80 m during period #4 (~60 days, Fig. 22d). Instead, relatively unmixed, although relatively light, TDW was observed at 270 m while waters at 80 m were either similar, even if more mixed, to those at 270 m or markedly different indicating for the first time the occurrence of mixed WMDW there, and hence the possible occurrence of less mixed WMDW along the slope in between. During period #5 (~250 days, Fig. 22e), similar comments can be made about TDW and WMDW at both 270 and 80 m. But LIW was also often encountered at both sites in more

or less mixed conditions. Denser WMDW might have outflown along the southern slope. During period #6 (~380 days, Fig. 22f) the LIW occurrence markedly reduced at 270 m and completely disappeared at 80 m. The overall densest TDW and maybe some WMDW were encountered at 270 m while the overall less-mixed WMDW was observed at 80 m, hence suggesting that denser WMDW were significantly outflowing in between.

The alternation of a MWs outflow mainly originated from either the western basin or the eastern one as suggested by the GE profiles is thus definitely demonstrated by the HCP time series that, additionally, document the large variability in all MWs amounts. Moored CTDs, possibly complemented by ship-handled CTDs operated along transects as often as possible, are clearly efficient, reliable and relatively simple instruments that are suitable for monitoring strategies and can provide significant information about such an outflow composition and variability in the long-term.

### 4.4. A two-layer approximation up to the sill

This subsection aims at checking, with relatively crude computations from the GE data, if differentiating light vs. dense (instead of intermediate vs. deep) MWs, can help explaining some of the current thoughts (such as the 90% LIW and 10% WMDW). Another aim is to help us better describing how a MW such as WMDW can reach the sill depth, hence to try improving our own understanding of the whole sea functioning.

The GIB data set indicates that, from east to west in the Alboran up to the sill, the mixing of all MWs does not especially increase while all associated isopycnals more and more tilt up southward. Close to the sill, let's say from ~5°15′W to ~5°40′W, it can be easily assumed that both the light MWs (WIW, LIW, upper-TDW) and the dense MWs (lower-TDW, WMDW) circulate significantly all across the strait, even if more or less homogeneously. More to the east, i.e. from ~4°30′W to ~5°00′W, this is expectedly not the case since, according to our personal thoughts, dense MWs are quite motionless while, according to our data analysis, they can be found just below AW in the south. The thermal wind equations for two homogeneous layers can thus be used to check if assuming an outflow composed of two (sets of) MWs as done by previous authors is supported by the GE data or not. When characterizing the light vs. dense MWs by mean values of density ($\rho_L$ vs. $\rho_D$), speed ($V_L$ vs. $V_D$) and amount, i.e. section area ($A_L$ vs. $A_D$), the slope of their interface is:

$$I_{LD} = f/g/(\rho_D - \rho_L)(\rho_D V_D - \rho_L V_L)$$

with $f$ the Coriolis parameter ($10^{-4}$ s$^{-1}$) and $g$ gravity (10 m s$^{-2}$), $I_{LD} < 0$ indicating a tilting up southward. These mean values must also satisfy the relationship:

$$V_L A_L + V_D A_D = Q$$

with $Q$ the outflow transport. Specifying $\rho$ values from the GE data (as displayed in particular by the $\theta$–$S$ diagrams), $A$ values from e.g. Fig. 3, and $Q$ from the literature allows computing $V_L$ and $V_D$ values, hence checking the light vs. dense MWs transports ($Q_L = V_L A_L$ vs. $Q_D = V_D A_D$).

We chose $\rho_L$ = 1 029.05 kg m$^{-3}$ and $\rho_D$ = 1 029.09 kg m$^{-3}$. We specified $A_L$ and $A_D$ from interfaces defined by $\rho_{LD}$ = 1 029.08 kg m$^{-3}$ for the light–dense MWs interface (slope = $I_{LD}$) and $\rho_{AM}$ = 1 028.75 kg m$^{-3}$ for the AW–MWs interface. We retained for $Q$ the most recent and generally accepted estimate of $0.7 \times 10^6$ m$^3$ s$^{-1}$ (Bryden et al. 1994). These assumptions and estimates are very crude but we checked what could be foreseen from the equations, i.e. that modifying realistically these values, hence changing $Q_L$ vs. $Q_D$, does not markedly change the inferred results. General distribution of $\rho_{LD}$ and $\rho_{AM}$ in Fig. 3 (as $\sigma_{LD}$ and $\sigma_{AM}$) also provides an overlook of both GIB1 and GIB2. Focusing on the transects east of the sill, note that (i) $\rho_{AM}$ is generally, but not always, tilting up northward, (ii) $\rho_{LD}$ is always tilting up southward with marked GIB1–GIB2 differences close to the sill, (iii) there, $A_D$ is relatively low during GIB1, (iv) $\rho_{LD}$ can parallel the southern slope.

Results (Table 2) first show that $Q_L/Q$ is 40–65% at 4°30′–5°00′W (35–60% for $Q_D/Q$) and 70–95% closer to the sill (5–30% for $Q_D/Q$). Assuming the transports conservation through the various $A_L$ and $A_D$ sections, results away from the sill lead, close to the sill, to unacceptable features such as inflowing MWs. Furthermore percentages of ~50% are unexpected from the literature, this confirms our thoughts that the 2-layer approximation is not valid away from the sill. Results close to the sill give % values that compare well with the currently assumed LIW to WMDW ratio of 9:1, which supports our idea that LIW and WMDW have not been differentiated up to now from the whole sets of light and dense MWs. It can be noted that relying on the $V_D$ and $A_D$ values close to the sill leads to $V_D$ values in the central Alboran of a few $10^{-3}$ m s$^{-1}$, which supports our hypothesis that the dense MWs in the subbasin are quite motionless. Results show marked differences between GIB1 and GIB2 since e.g. $Q_L/Q$ is markedly larger during GIB1 (84–97%) than during GIB2 (70–80%), which supports our initial remark that there are no reasons to assume a constant ratio between light and dense MWs, and that this ratio can markedly change. Particularly during GIB2 when $Q_D$ is relatively large, the interface found at more than 300 m away from the sill can be found at less than 200 m near the sill ($Z_{min}$, Table 2). Also note that a relatively low $Q_D$ east of the sill, as during GIB1 vs. GIB2, is consistent with relatively low $\sigma$ after the sill, due to the AW mixing at the sill. Finally, the maximum $I_{LD}$ values (~$3 \times 10^{-2}$) are close to that of $5 \times 10^{-2}$ inferred from Fig. 3 for the Moroccan continental slope. At the sill, dense MWs can thus easily flow along the southern slope and even over the shelf, hence possibly leading to $\sigma$ values larger at 80 m than at 270 m.

**Table 2**
The slope of the light–dense MWs interface $I_{LD}$ for the GIB1 and GIB2 transects east of the sill is inferred from a linear fit of $\sigma$ = 29.08 kg m$^{-3}$; specified characteristics are its minimum immersion ($Z_{min}$), vertical range ($\Delta Z$), width ($Y$) and numerical value. The $A_L$ and $A_D$ sections areas are inferred from bathymetric profiles (Fig. 3) and from a AW–MWs interface identified with $\sigma$ = 28.75 kg m$^{-3}$. $V_L$, $V_D$, $Q_L$ and $Q_D$ are computed as specified in the text.

| | | $I_{LD}$ ($Z_{min}$, $\Delta Z$, $Y$) m/m/nm ($10^{-3}$) | $A_L$ $10^6$ m$^2$ | $A_D$ $10^6$ m$^2$ | $V_L$ $10^{-2}$ m s$^{-1}$ | $V_D$ $10^{-2}$ m s$^{-1}$ | $Q_L/Q$ (%) | $Q_D/Q$ (%) |
|---|---|---|---|---|---|---|---|---|
| 4°30′ | GIB1 | 360/60/66.0 (0.5) | 35.5 | 71.0 | 0.8 | 0.6 | 41 | 59 |
| | GIB2 | 380/180/66.0 (1.4) | 40.0 | 62.2 | 1.1 | 0.4 | 63 | 37 |
| 5°00′ | GIB1 | 300/120/45.6 (1.4) | 22.8 | 17.9 | 2.0 | 1.3 | 65 | 35 |
| | GIB2 | 300/120/45.6 (1.4) | 19.8 | 17.9 | 2.2 | 1.5 | 62 | 38 |
| 5°15′ | GIB1 | 300/200/15.0 (7) | 12.9 | 6.3 | 4.6 | 1.8 | 84 | 16 |
| | GIB2 | 320/120/15.0 (4) | 11.8 | 7.0 | 4.3 | 2.7 | 72 | 28 |
| 5°30′ | GIB1 | 360/240/4.8 (27) | 5.1 | 0.8 | 13 | 3 | 97 | 3 |
| | GIB2 | 180/320/5.4 (32) | 2.7 | 1.8 | 21 | 8 | 80 | 20 |
| 5°40′ | GIB1 | 320/180/3.0 (32) | 3.2 | 0.4 | 21 | 8 | 95 | 5 |
| | GIB2 | 220/160/5.4 (16) | 2.3 | 1.3 | 22 | 15 | 71 | 29 |

### 4.5. Another concept of the outflow

Describing our understanding of the outflow is simplified by considering the sea as a unique basin transforming AW into light and dense waters (LW, DW). Most of the DW formed in a shallow (2000 m) northern region reaches the bottom and amasses locally before spreading, cascading and circulating alongslope, as the whole outflow itself along the Iberian slope. The key point is that any cascading of dense DW uplifts less dense DW with the major consequence that, at depths <1500 m in the Alboran subbasin in particular, the less dense uppermost DW does not circulate significantly.

Without any LW (in a simple idealistic case), or with DW formed in relatively large amount, the DW upper part is relatively unmixed, it easily reaches the sill depth (~300 m) and outflows there, be rotation considered or not (rotation just shifting the DW outflow northward). Such a situation was observed at the beginning of the first HCP period and we propose to consider it as an overflow (not outflow) of relatively homogeneous DW.

LW formed in relatively large amount amasses over DW before spreading and circulating alongslope, hence easily outflowing through the strait. A large LW amount in the strait surroundings can prevent any DW from outflowing in unmixed conditions (as during the third HCP period).

In general, LW and DW are formed in significant amounts during several years so that both have to outflow at Gibraltar. In the sea, AW and LW flow together counterclockwise alongslope, leading to a reduced mixing. Along its route in the northern Alboran, LW still does not strongly mix with AW, maybe because AW flows in the south so that its amount in the north is reduced (see Figs. 2 and 3), even though AW generally describes one or two anticyclonic gyres there (Millot, 1999). On the contrary, uplifted DW is in direct contact with AW in the south of the basin and it tends to move westward, i.e. against AW for a while. Furthermore the AW flow is very turbulent there (the Algerian Eddies), no doubts that DW in the southern Alboran is markedly mixed with AW.

Since LW outflows more easily than DW, $V_L >> V_D$ and both the small $(\rho_D - \rho_L)$ value and rotation lead to a marked tilting up southward of $I_{LD}$ in the strait surroundings. Assuming a constant $Q_L$, the larger $V_L$ the larger $I_{LD}$ and the easier the way in which DW is brought up to the sill depth. In an extreme situation (large $Q_L$, large $|I_{LD}|$), DW is found on the southern slope and shelf while LW is found at the sill (as during the second HCP period). Whatever the case, LW and DW outflow side by side, being more juxtaposed than superposed and then easily mix individually with AW.

Just west of the sill, this leads to a LW and a DW juxtaposed suboutflows that are continuously stratified and that will then cascade separately alongslope. The LW suboutflow remains along the northern slope while the DW suboutflow first cascades from the southern slope towards the central part of the strait before cascading along the northern slope too. The LW and DW suboutflows are then identified as superposed LW and DW veins. The outflow characteristics downstream from the strait depend on its characteristics upstream and, more importantly, on the AW characteristics in the sill surroundings.

## 5. Conclusion

Considering the major differences between the current thoughts and our personal ones (Section 1), we have recently undertaken a series of analyses about the Strait of Gibraltar (Section 1.2.3). We first proposed herein (Section 2) a re-analysis of CTD profiles collected in 1985–1986 during several campaigns (GIB1, GIB2, LYNCH-702-86) of the Gibraltar Experiment that we consider as extremely valuable and reliable. We then proposed (Section 3) the analysis of two four-year CTD time series collected in 2003–2007 close to Camarinal Sill South (270 m) and on the nearby Moroccan shelf (80 m) as part of the Hydro-Changes CIESM Programme that we initiated in the early 2000s.

We showed that all four major MWs (WIW, LIW, TDW, WMDW) can be identified in the Alboran subbasin, hence indicating that each of the two basins of the sea produces significant amounts of both intermediate and deep waters. In the sill surroundings, we prefer considering a set of light MWs (WIW, LIW, upper-TDW) and a set of dense MWs (lower-TDW, WMDW). The former circulates alongslope counterclockwise and is thus located along the northern slope. The latter is mainly uplifted and quite motionless, being possibly found just below AW along the southern slope. We also showed that any of the MWs, including LIW and WMDW, can be more or less negligible components of the outflow. The MWs outflow can mainly originate from either the eastern or the western basins, as indicated by the eastern (vs. western) dominance encountered during GIB1 (vs. GIB2) and the first (vs. second) half of the HCP experiment.

We identified situations (first HCP period) during which the dense MWs are relatively unmixed and flow mainly at the sill (not on the southern slope and shelf), which could be associated with what we have called an overflow. We also identified situations (third period) during which the outflow is mainly composed of light MWs. More generally, both light and dense MWs outflow together, since the western and/or the eastern basin produce, on average, both of them in significant amounts. We have shown (Section 4.4) that a two-layer assumption and rotation can allow specifying the light vs. dense outflow characteristics just east of the sill (~5°15′W to 5°40′W), hence supporting the GE data to demonstrate that the light–dense MWs interface can easily parallel the southern slope. Dense MWs can thus be found on the Moroccan shelf, being there eventually denser than at the sill (second HCP period). We have specified some aspects of the short-term, seasonal and long-term variabilities of the outflow characteristics (Sections 4.1–4.3).

In general, when all four MWs can be identified east of the sill, they come to be, near to the sill, less superposed than juxtaposed (the denser the more to the south) and they mix individually with AW. As demonstrated by the GIB and LYNCH data west of the sill, this leads to a series of juxtaposed suboutflows that will then cascade individually, hence regularly coming to be superposed as veins flowing northward along the Iberian slope. The outflow splitting into veins is thus due mainly to the outflow composition east of the sill, not to bathymetric features west of the sill. But the veins characteristics 100–200 km from the strait depend more on the AW composition (NACW vs. SAW) and distribution in the sill surroundings than on the MWs characteristics in the sea. It is thus illusory to characterize the veins by specific hydrographic values, furthermore fortnightly and seasonal signals are created in the sill surroundings.

We hope that the hydrographic data analysis made herein on the basis of personal thoughts will motivate further more sophisticated studies.

## Acknowledgements

I thank (i) Frédéric Briand, general director of CIESM (The Mediterranean Science Commission) for his initial and unflinching support for the Hydro-Changes Programme on which data part of this paper is based, (ii) Youssef Tber for his enthusiasm in initiating the monitoring of the study area from Morocco, (iii) the SHOMAR (Service Hydrographique et Océanographique de la Marine Royale du Maroc) for its efficient logistics, (iv) Jean-Luc Fuda and Gilles Rougier for their help during the servicing, (v) Julio Candela for providing me with his data for the tide at Tarifa, (vi) Cathy and Rex Reno for their help in improving the English of a preliminary version of

the paper and Paul Robertson for providing valuable comments about the writing, (vii) the Université de la Méditerranée and Bernard Tramier from TOTAL-ELF for their financial support, (viii) AANDERAA for having lend me the currentmeter, (ix) the crew of S/V *Ailes et Iles*.

## References

Allain, C., 1964. L'hydrologie et les courants du Détroit de Gibraltar pendant l'été de 1959. Revue des Travaux de l'Institut des Pêches Maritimes 28, 1–99.
Ambar, I., Howe, M.R., 1979a. Observations of the Mediterranean outflow – I. mixing in the Mediterranean outflow. Deep-Sea Research I 26A, 535–554.
Ambar, I., Howe, M.R., 1979b. Observations of the Mediterranean Outflow – II. The deep circulation in the vicinity of the Gulf of Cadiz. Deep-Sea Research I 26A, 555–568.
Ambar, I., 1983. A shallow core of Mediterranean Water off Western Portugal. Deep-Sea Research I 30, 677–680.
Ambar, I., Armi, L., Bower, A., Ferreira, T., 1999. Some aspects of time variability of the Mediterranean Water off South Portugal. Deep-Sea Research I 46, 1109–1136.
Ambar, I., Serra, N., Brogueira, M.J., Cabeçadas, G., Abrantes, F., Freitas, P., Gonçalves, C., Gonzales, N., 2002. Physical, chemical and sedimentological aspects of the Mediterranean outflow off Iberia. Deep-Sea Research II 49, 4163–4177.
Baringer, M., Price, J., 1997. Mixing and spreading of the Mediterranean outflow. Journal of Physical Oceanography 27, 1654–1677.
Baringer, M., Price, J., 1999. A review of the physical oceanography of the Mediterranean outflow. Marine Geology 155, 63–82.
Béthoux, J.P., Gentili, B., Raunet, J., Tailliez, D., 1990. Warming trend in the Western Mediterranean Deep Water. Nature 347, 660–662.
Borenäs, K.M., Wahlin, A.K., Ambar, I., Serra, N., 2002. The Mediterranean outflow splitting – a comparison between theoretical models and Canigo data. Deep-Sea Research II 49, 4195–4205.
Bray, N.A., Ochoa, J., Kinder, T.H., 1995. The role of the interface in exchange through the Strait of Gibraltar. Journal of Geophysical Research 100 (C6), 10755–10776.
Bryden, H.L., Millard, R.C., Porter, D.L., 1978. CTD observations in the western Mediterranean sea during cruise 118, Leg 2 of R/V Chain, February 1975. Woodw Hole Oceanographic Institution Technical Report, 78–26, March, 38 pp.
Bryden, H.L., Stommel, H.M., 1982. Origin of the Mediterranean outflow. Journal of Marine Research 40 (Suppl.), 55–71.
Bryden, H.L., Stommel, H.M., 1984. Limiting processes that determine basic features of the circulation in the Mediterranean Sea. Oceanologica Acta 7, 289–296.
Bryden, H.L., Kinder, T.H., 1991. Recent progress in strait dynamics. Reviews of Geophysics (Supp.), 617–631.
Bryden, H.L., Candela, J., Kinder, T.H., 1994. Exchange through the Strait of Gibraltar. Progress in Oceanography 33, 201–248.
Candela, J., Winant, C., Ruiz, A., 1990. Tides in the Strait of Gibraltar. Journal of Geophysical Research 95 (C5), 7313–7335.
Davies, P.A., Guo, Y., Rotenberg, E., 2002. Laboratory model studies of Mediterranean outflow adjustment in the Gulf fo Cadiz. Deep-Sea Research II 49, 4207–4223.
Fuda, J.-L., Font, J., Garcia-Lafuente, J., Gasparini, G.-P., Millot, C., and others, 2007. Hydrochanges: first results and perspectives. Rapports de la Commission Internationale pour l'Exploration Scientifique de la mer Méditerranée. 38, 27.
Gascard, J.C., Richez, C., 1985. Water masses and circulation in the western Alboran Sea and in the Straits of Gibraltar. Progress in Oceanography 15, 157–216.
Howe, M., Abdullah, M., Deetae, S., 1974. An interpretation of the double T–S maxima in the Mediterranean outflow using chemical tracers. Journal of Marine Research 32 (3), 377–386.
Johnson, J., Ambar, I., Serra, N., Stevens, I., 2002. Comparative studies of the spreading of Mediterranean water through the Gulf of Cadiz. Deep-Sea Research II 49, 4179–4193.
Kinder, T.H., Parrilla, G., 1987. Yes, some of the Mediterranean outflow does come from great depths. Journal of Geophysical Research 92 (C3), 2901–2906.
Lacombe, H., Richez, C., 1982. The regime of the Straits of Gibraltar. In: Nihoul, J.C.J. (Ed.), Hydrodynamics of Semi-Enclosed Seas. Elsevier, Amsterdam, pp. 13–74.
Madelain, F., 1970. Influence de la topographie du fond sur l'écoulement Mediterranéen entre le Détroit de Gibraltar et le Cap Saint-Vincent. Cahiers Océanographiques 22, 43–61.
MEDAR Group, 2002. MEDATLAS/2002 database. Mediterranean and Black Sea database of temperature salinity and bio-chemical parameters. Climatological Atlas. IFREMER Edition (4 CDroms).
Millot, C., 1999. Circulation in the Western Mediterranean sea. Journal of March Systems 20 (1–4), 423–442.
Millot, C., 2007. Interannual salinification of the Mediterranean inflow. Geophysical Research Letters, 34, L21069. doi: 10.1029/2007/GL031179. Available from: <www.ifremer.fr/lobtln>.
Millot, C., 2008. Short-term variability of the Mediterranean in- and out-flows. Geophysical Research Letters, 35, L15603. doi: 10.1029/2008/GL033762. Available from: <www.ifremer.fr/lobtln>.
Millot, C., Taupier-Letage, I., (2005a). Circulation in the Mediterranean Sea. In: The Handbook of Environmental Chemistry, Water Pollution, Part K, vol.5, Springer-Verlag, Berlin-Heidelberg. . pp. 29–66. doi: 10.1007/b107143. Available from: <www.ifremer.fr/lobtln>.
Millot, C., Taupier-Letage, I., 2005b. Additional evidence of LIW entrainment across the Algerian Basin by mesoscale eddies and not by a permanent westward-flowing vein. Progress in Oceanography 66, 231–250. Available from: <www.ifremer.fr/lobtln>.
Millot, C., Candela, J., Fuda, J.-L., Tber, Y., 2006. Large warming and salinification of the Mediterranean outflow due to changes in its composition. Deep-Sea Research 53/4, 656–666. doi:10.1016/j.dsr.2005.12.017. Available from: <www.ifremer.fr/lobtln>.
Ochoa, J., Bray, N.A., 1991. Water mass exchange in the Gulf of Cadix. Deep-Sea Research 38 (Suppl. 1), 465–503.
Parrilla, G., Kinder, T.H., Bray, N.A., 1989. Hidrologia del Agua Mediterranea en el Estrecho de Gibraltar durante el Experimento Gibraltar (Octubre, 1985–Octubre, 1986). In: Almazan, J.L., Bryden, H., Kinder, T., Parrilla, G. (Eds.), Seminario sobre la oceanografia fisica del Estrecho de Gibraltar, Madrid 24–28 Octubre, 1988. pp. 95–121.
Pettigrew, N.R., 1989. Direct measurements of the flow of Western Mediterranean Deep Water over the Gibraltar sill. Journal of Geophysical Research 94 (C12), 18089–18093.
Roether, W., Manca, B., Klein, B., Bregant, D., Georgopoulos, D., Beitzl, V., Kova, V., Luchetta, A., 1996. Recent changes in Eastern Mediterranean Deep Waters. Science 271, 333–335.
Sannino, G., Bargagli, A., Artale, V., 2002. Numerical modeling of the mean exchange through the Strait of Gibraltar. Journal of Geophysical Research 107 (C8), 3094. doi:10.1029/2001JC000929.
Serra, N., Ambar, I., 2002. Eddy generation in the Mediterranean Undercurrent. Deep-Sea Research II 49 (19), 4225–4243.
Siedler, G., 1968. The frequency distribution of water types in the outflow region of straits. Kieler Meeresforschung 24, 59–65.
Sparnocchia, S., Gasparini, G.P., Astraldi, M., Borghini, M., Pistek, P., 1999. Dynamics and mixing of the Eastern Mediterranean Outflow in the Tyrrhenian Basin. Journal of March Systems 20, 301–317.
Vargas-Yanez, M., Ramirez, T., Cortes, D., Sebastian, M., 2002. Warming trends in the continental shelf of Malaga Bay (Alboran Sea). Geophysical Research Letters 29 (22), 2082. doi:10.1029/2002GL015306.
Vargas, J.M., García-Lafuente, J., Candela, J., Sánchez, A.J., 2006. Fortnightly and monthly variability of the exchange through the Strait of Gibraltar. Progress in Oceanography. doi:10.1016/j.pocean.2006.07.001.
Wesson, J.C., Gregg, M.C., 1994. Mixing at Camarinal Sill in the strait of Gibralter. Journal of Geophysical Research 99 (C3), 9847–9878.
Wu, W., Danabasoglu, G., Large, W.G., 2007. On the effects of parameterized Mediterranean overflow on North Atlantic ocean circulation and climate. Ocean Modelling 19 (1-2), 31–52.
Zenk, W., 1975. On the origin of the intermediate double maxima in T/S profiles from the North Atlantic. Meteor Forschungsergebnisse A 16, 35–43.